4-5-2018

An insoluble iron complex coated cathode enhances direct electron uptake by Rhodopseudomonas palustris TIE-1

Karthikeyan Rengasamy

Tahina Ranaivoarisoa

Rajesh Singh

Arpita Bose
abose@wustl.edu

An Insoluble Iron Complex Coated Cathode Enhances Direct Electron Uptake by *Rhodopseudomonas palustris* TIE-1

Karthikeyan Rengasamy, Tahina Ranaivoarisoa, Rajesh Singh, Arpita Bose*

Department of Biology, Washington University in Saint Louis, St. Louis, MO, 63130, USA.

Abstract

Microbial electrosynthesis (MES) is a promising bioelectrochemical approach to produce biochemicals. A previous study showed that *Rhodopseudomonas palustris* TIE-1 can directly use poised electrodes as electron donors for photoautotrophic growth at cathodic potentials that avoid electrolytic H_2 production (photoelectroautotrophy). To make TIE-1 an effective biocatalyst for MES, we need to improve its electron uptake ability and growth under photoelectroautotrophic conditions. Because TIE-1 interacts with various forms of iron while using it as a source of electrons for photoautotrophy (photoferroautotrophy), we tested the ability of iron-based redox mediators to enhance direct electron uptake. Our data show that soluble iron cannot act as a redox mediator for electron uptake by TIE-1 from a cathode poised at +100mV vs. Standard Hydrogen electrode. We then tested whether an immobilized iron-based redox mediator Prussian blue (PB) can enhance electron uptake by TIE-1. Chronoamperometry indicates that cathodic current uptake by TIE-1 increased from 1.47 ± 0.04 to 5.6 ± 0.09 $\mu A/cm^2$ (3.8 times). Overall, our data show that immobilized PB can enhances direct electron uptake by TIE-1.

Keywords: Rhodopseudomonas palustris TIE-1; Microbial electrosynthesis; Photoelectroautotrophy; Prussian blue; Electron uptake.

*Corresponding author email: abose@wustl.edu, Tel: +1-314-935-7313

1. Introduction

Microbial electrochemical systems (MECs) use microbes to catalyze biochemical reactions at the electrode-microbe interface [1,2]. Recent research suggests that microbial electrosynthesis (MES) is an attractive approach to compensate for fossil fuel shortage and to mitigate climate change [3,4]. In MES, electrically driven microorganisms (e.g., cathodophilic- or metal-oxidizing microorganisms) are used as biocatalysts to convert CO_2 to value-added chemicals, biomass or biogas using a poised cathode potential [2-8]. Under a poised potential, extracellular electron transfer between the cathode and microbes can occur in the following ways: (1) Electron transfer (ET) through H_2, which is externally supplied from the electrolyzer, (2) ET through cathodically produced H_2 (self-mediated), (3) Direct ET to drive microbial CO_2 fixation [9]. Also, the production of biochemicals from CO_2 is directly linked to the quantity of electrical energy supplied by the cathodically poised electrode [5-9].

Acetogens and methanogens are widely employed as microbial catalysts in MES for biochemical production from CO_2 [10-12]. Under electroautotrophic conditions, both acetogens and methanogens can perform mediated electron transfer (MET) using cathodically produced H_2 as electron mediator (self-mediator) to generate bio-chemicals. The poised cathode potentials lower than -590 mV vs. Standard Hydrogen Electrode (SHE) (or more negative potentials) can favor MET due to the production of H_2. H_2 even at low quantities can act as an electron mediator between the electrode and microbes [1,13,14]. Electrodes poised at low potentials of -1500 mV vs. SHE can also undergo MET due to the production of formate, which can act as an electron mediator in MES by lithoautotrophic microorganisms (e.g., *Ralstonia eutropha)* [15]. Although high levels of electron uptake can be achieved by acetogens/methanogens, the main issue associated with using them for MES is that the process requires high energy input (i.e., a more negative potential), thus increasing the cost of the biochemicals produced using this strategy [16-19].

Rhodopseudomonas palustris TIE-1 is an iron-oxidizing photoautotrophic microorganism that can fix CO_2 in the presence of light by using ferrous iron (Fe(II)) as a source of electrons (photoferroautotrophy) [20,21]. Bose *et al.* [22] demonstrated that TIE-1 can uptake electrons (~1.5 $\mu A/cm^2$) from a solid graphite electrode under low electrical energy input (+100 mV vs. SHE). Bose *et al*. [22] also showed that light enhances current uptake by TIE-1. The low energy input requirement, the use of light, the metabolic versatility and the genetic tractability of TIE-1 represent major advantages for its use in future MES applications. However, for this, we need to improve its electron uptake ability and its growth under photoelectroautotrophic conditions. Although Bose *et al.* [22] suggested that direct electron uptake is the most likely mechanism by which TIE-1 accepts electrons from an electrode poised at +100 mV vs. SHE (based on electrochemical calculations) [22], Doud and Angenent [23] suggested that ferrous iron could act as a soluble redox mediator in these experiments. Doud and Angenent [23] suggested that TIE-1 was accepting electrons via indirect electron transfer where the electrode reduced ferric iron back to ferrous iron, thus making it available to TIE-1 to be used for photoferroautotrophy. The potential used by Doud and Angenent was +20 mV vs. SHE, which is different from that reported by Bose *et al.* (+100 mV vs. SHE) [22,23]. Doud and Angenent [22] also showed that increasing light input improved electron uptake by TIE-1 in an uncoupled bioelectrochemical reactor where phototrophic oxidation of Fe(II) chelated with Nitrilotriacetate (NTA) by TIE-1 produced Fe(III)-NTA. The poised electrode (+20 mV vs.

SHE) reduced this back to Fe(II)-NTA [23]. This is a reaction that can occur because the Fe(III)-NTA/Fe(II)-NTA redox couple has a reduction potential of ~ +400 mV vs. SHE at circumneutral pH [24]. In contrast to studies of indirect electron uptake reported by Doud and Angenent [23], here we wanted to test the effect of addition of unchelated Fe(II) on direct electron uptake by TIE-1 from electrodes poised at +100 mV vs. SHE as reported by Bose *et al.* [22]. Our results suggest that soluble Fe(II) cannot act as a redox mediator for electron uptake by TIE-1 and is unable to enhance cathodic current uptake at +100 mV vs. SHE. In search of a redox mediator that enhances direct electron uptake by TIE-1, we decided to use an immobilized iron-based redox mediator called Prussian Blue (PB). PB is a reversible ferrous-ferric polynuclear chemical complex that we electrodeposited as a film on graphite cathodes, and covered with a biocompatible chitosan layer.

The use of PB for our study was motivated by previous reports where graphite cathodes modified with Fe(III) aided oxygen reduction in microbial fuel cells by acting as a redox mediator [25,26]. Also, redox mediator modified electrodes improve electron transfer in biosensors; during electrocatalysis; in charge storage devices; and for electrochromism [27]. Among these redox mediators, Prussian blue (PB) complex {iron(III) hexacyanoferrate} is used very commonly in electrochemical biosensors [28-30]. Interestingly, an open framework structure of PB analogues allows rapid insertion and extraction of multivalent cations. PB is used as a low-cost cathode material (<$1 per Kg) in microbial batteries due to its reversible characteristic for long-term applications [29].

Here, we report that TIE-1 can accept more electrons from cathodes coated with PB, representing an inexpensive method for increasing electron uptake and the production of biomass as a product of microbial electrosynthesis. We performed electrochemical analyses to measure current uptake, electrochemical activity, and electron or charge transfer resistance across the electrode-microbe (TIE-1) interface of the unmodified and modified electrodes during photoelectroautotrophic growth. The results show that extracellular electron uptake of TIE-1 increased up to 3.8 times in the presence of the immobilized ET redox mediator, Prussian Blue.

2. Experimental

2.1. Inoculum and Bioelectrochemical cell (BEC) setup

Electron uptake (EU) experiments with TIE-1 were carried out in a seal-type single chamber electrochemical cell (C001 Seal Electrolytic cell, Xi'an Yima Opto-electrical Technology Com., Ltd, China). 10 mL of cells pre-grown in Freshwater (FW) [31] medium containing H_2 as an electron donor and 22 mM sodium bicarbonate were inoculated in 70 mL of FW medium to achieve a final OD_{660} of ~0.01. This was followed by gas exchange for 20 mins with N_2/CO_2 (80%:20%), and the final headspace pressure was set as 7 psi. All photoelectroautotrophic growth experiments were replicated (n=3) at 26 °C under continuous infrared light (illumination) unless noted otherwise (Fig. S1). We performed two sets of experiments: 1) Those with the addition of $FeCl_2$ using unmodified graphite electrodes, and 2) Those using the electrode modified with PB.

2.2. Bioelectrochemical experiments with $FeCl_2$

Electron uptake of TIE-1 was performed by the addition of $FeCl_2$ (referred to as soluble Fe(II)) with poised electrodes in the seal type electrochemical cell. Here, **s**pectroscopically pure graphite rods (GR, 5.149 cm^2, SPI supplies, USA) served as the working electrode, Pt

foil as the counter electrode and Ag/AgCl as the reference electrode. All potential values are reported with respect to the Standard Hydrogen Electrode potential (SHE). All electrochemical experiments were carried out using the Gamry electrochemical workstation (Gamry Multichannel potentiostat, USA). To investigate the dissolved Fe(II) during the EU experiment, 6.32± 0.02 mM of $FeCl_2$ was added to FW medium in the presence or absence of TIE-1. EU by TIE-1 was measured in terms of current by chronoamperometry (CA) method at a poised potential of +100 mV vs. SHE for 152 h. Cyclic voltammetry (CV) characteristics of initial (0 h) and final (152 h) FW medium was analyzed to understand the effect of Fe(II) addition. Further, a colorimetric Ferrozine based assay was used to determine Fe(II) oxidation in the bioreactor as reported previously [20]. Finally, both the electrode surface and the spent salt medium containing planktonic cells was analyzed by JEOL JSM-7001 LVF field emission scanning electron microscopy (FE-SEM). In which, a piece (5 mm) of the graphite cathode or the spent medium from the bioreactors was fixed in 2% glutaraldehyde in 100 mM sodium cacodylate buffer for 5 h. Fixed graphite cathodes were gently rinsed with 100 mM cacodylate buffer followed by dehydration washing with a series of ethanol for 10 mins (30, 50, 70 and 100%). Finally, the dehydrated microbial cathode samples were sputter coated with a thin gold layer to perform SEM imaging and Electron Dispersive Spectroscopy (EDS).

2.3. Electrochemical modification of graphite cathodes

Graphite rods (GR, 5.149 cm^2, spectroscopically pure graphite, SPI supplies) were used as substrate electrodes for Prussian blue (PB, $Fe_4[Fe(CN)_6]_3 \cdot xH_2O$) electrodeposition in a three-electrode configured electrochemical cell as described above. Electrochemical deposition was performed using a bath containing 10 mM $K_3[Fe(CN)_6]$, 10 mM $FeCl_3.6H_2O$ and 10 mM HCl (Fig. S1). Electrodeposition of PB was carried out at a constant potential of -300 mV for 180 seconds using the Gamry electrochemical workstation. The modified graphite electrodes were cyclically scanned between -0.1 V to 1.4 V at 50 mV/s in 0.1 M KCl for >30 times to maintain the electroneutrality and to enhance the stability of the voltammetric peaks [32]. Further, the PB-graphite electrodes were dip-coated with 0.5% chitosan solution and dried under N_2 gas. Prior to use, the PB-chitosan (PB/Chit) coated graphite electrodes were immersed in deionized water for 4 h and gently rinsed to remove soluble ions on the electrode surface. In order to compare the effect of the PB modification on electron uptake by TIE-1, the working electrode was configured as an unmodified graphite rod (GR), a graphite rod coated with 0.5% chitosan (GR/Chit), and a graphite rod modified with PB and 0.5% chitosan (GR/PB/Chit). PB modified electrodes with no chitosan were not tested because of the possible detachment of the PB film in the bioreactor. Surface analysis of as-deposited PB complex was confirmed with SEM, EDS, X-ray photoelectron spectroscopy (Physical Electronics® 5000 VersaProbe II Scanning ESCA (XPS) Microprobe), and the thickness of PB layer was measured with a profilometer (KLA - Tencor Alpha - Step D - 100 Profilometer).

2.4. Bioelectrochemical experiment with modified electrodes

To measure the current response, Chronoamperometry (CA) analysis was conducted for 130 h at the constant applied potential of +100 mV. The optical density at 660 nm (Hand held OD scanner BEH100, Bug Lab, CA 94521, USA; Measures 0-30 OD units without needing a dilution) was measured during the electron uptake experiment with TIE-1 at 0 h

and 130 h. Cyclic voltammetry (CV) and differential pulse voltammetry (DPV) of TIE-1 on different graphite electrodes was performed using a potential scan from -100 mV to +900 mV. The midpoint redox potential from CV was calculated from the average of E'_{pa} (anodic peak potential) and E'_{pc} (cathodic peak potential), i.e., $(E'_{pa}+E'_{pc})/2$. Electrochemical impedance spectroscopy (EIS) was performed at +100 mV in the frequency range of 1 MHz to 10 mHz with a perturbation voltage of 10 mV. Further, the obtained EIS data were fitted by ZSimpwin 3.10 software (Echem, US) with the appropriate equivalent circuit to derive the value of circuit components. Potentiodynamic polarization (Tafel) of electrodes with biofilms were performed from -250 mV (cathodic reduction) to + 250 mV (anodic oxidation) at 0.5 mV/s. Tafel parameters was derived from extrapolating the linear portions of logarithmic current (anodic and cathodic region) versus potential back towards their intersection. Field Emission-SEM was used to characterize the microbial attachment on graphite cathodes, and the sample preparation for imaging was as described above.

3. Results and discussion

3.1. Electrotrophic characteristics of TIE-1 in response to addition of soluble Fe(II)

To understand the effect of soluble Fe(II) on electron uptake from poised electrodes (solid electron donor) by TIE-1, an unmodified graphite cathode was poised at +100 mV vs. SHE in presence of 6.32 ± 0.02 mM soluble $FeCl_2$ under both abiotic (No cells) and biotic (TIE-1 cells) conditions for 152 h. On addition of $FeCl_2$, the cathodic current changed to anodic current (Fig. 1a). The peak anodic current was noted for the abiotic ($FeCl_2$ only) and biotic systems ($FeCl_2$ + TIE-1) as 21.18 ± 2.2 μA/cm^2 (total current, 3.498 ± 0.28 mA h) and 17.61 ± 1.3 μA/cm^2 (2.594 ± 0.11 mA h), respectively (Fig. 1a, b).

"Here Fig. 1"

This effect was clearly observed from the cyclic voltammetry of both the abiotic ($FeCl_2$) and biotic ($FeCl_2$ + TIE-1) systems on 0 h and 152 h at the potential of +100 mV (Fig. 1c, d). This confirms that the oxidation current of Fe(II) occurs at the peak potentials around 0.3 and 0.1 V, and supports electrochemical oxidation of Fe(II) to Fe(III) during the chronoamperometry condition. Further, the potential at 0.3 V (Fig. 1c) in the presence of $FeCl_2$ (at 0 h) shows the maximum current of 300 μA/cm^2 which is a significant oxidative peak. This peak current was lowered to around 144 μA/cm^2 at 152 h (difference 154 μA/cm2). The change in the magnitude of the oxidation current at two intervals (0 h and 152 h) indicates the electrochemical oxidation of Fe(II) to Fe(III). Moreover, in the abiotic system, the change in anodic or oxidation current was 154 ± 7 μA/cm^2 compared to 105 ± 16 μA/cm^2 in the biotic system at the interval of 0 - 152 h. Overall, the presence of TIE-1 cells lowers the observed anodic current. This confirms that the electrode mediates Fe(II) oxidation. This effect is perhaps due to the continued ability of TIE-1 cells to directly uptake electrons from the poised cathode, thus competing for the electrode surface. Chronoamperometry on biotic graphite electrodes with no added Fe(II) confirms that TIE-1 accepts electrons from unmodified electrodes as reported previously (-1.39 ± 0.02 μA/cm^2; Fig. 1a) [21]. SEM – EDS on both the abiotic and biotic reactor electrode surface as well as the spent medium showed the presence of iron oxides similar to Ferrihydrite (Fig. 2, Fig. S2, Fig. S3, Fig. S4). Fig. S3 shows the SEM image of spent medium containing

planktonic cells with sheet like Ferrihydrite formation in dissolved Fe(II) reactor (TIE-1→ $FeCl_2$, biotic system), and the elemental map confirms the oxides of iron surrounding TIE-1 cells. In the biotic system, the competition between Fe(II) and TIE-1 for the electrode surface was corroborated by SEM imaging of the BECs where TIE-1 cells were exposed to both a poised cathode and Fe(II) ($FeCl_2$+ TIE-1) (Fig. 2a-a' and Fig S2a-b). This competition between TIE-1 and Fe(II) for the electrode surface is perhaps due to electrochemical oxidation of Fe(II) and photoelectroautotrophy by TIE-1 occurring simultaneously on the poised electrode (cathode) surface. SEM images show that TIE-1 cells attach to areas devoid of iron oxides (Fig. 2a-a' and Fig S2a-b).

In a parallel experiment, we grew TIE-1 cells in poised reactors for 77 h before Fe(II) addition (TIE-1 → $FeCl_2$). SEM images of these electrodes show that cells already attached to the graphite electrodes get coated with iron oxides post Fe(II) addition (Fig. 2b, b'). Overall these data suggest that Fe(II) gets oxidized by an electrode poised at +100 mV vs. SHE. These data also indicate that TIE-1 and Fe(II) compete for the electrode surface for access to electrons. This is because the electrochemical oxidation of Fe(II) produces ferrihydrite (oxides of Fe(III)) on the electrode surface, which limits the accessibility of electrons to TIE-1. Ferrozine assays on abiotic and biotic reactors show that Fe(II) gets oxidized to Fe(III) in both cases (Table S1). Further, the electrochemical oxidation of Fe(II) at 0.1 V was also supported by the Ferrozine assay in which 19% Fe(II) was electrochemically oxidized to Fe(III). Due to this oxidation, the Fe(II) concentration was lowered to 81% (at 152 h) during chronoamperometry at 0.1V (Table S1). Chronoamperometry and Ferrozine assay indicate that there is a lower concentration of Fe(II) from the electrolyte due to electrochemical oxidation at 152 h. This effect was supported by the magnitudes of maximum peak current at two intervals from cyclic voltammetry (Fig. 1c, d). In the biotic reactors, 36% of the added Fe(II) is oxidized while in the abiotic reactors 19% of the added Fe(II) is oxidized. The higher Fe(II) oxidation in the biotic reactor is due to the concurrent effects of photoferroautotrophy and abiotic Fe(II) oxidation by the electrodes. It's notable that complete Fe(II) oxidation is not observed in the biotic reactors even after 152 h of incubation suggesting that TIE-1 is using both the electrodes (photoelectroautotrophic process) and Fe(II) (photoferroautotrophic process) for electrons. These data clearly show that added Fe(II) cannot serve as a redox mediator to enhance cathodic electron uptake by TIE-1. In fact, Fe(II) competes with TIE-1 for the electrode surface as a source of electrons.

"Here Fig. 2"

3.2. Characterization of the Prussian blue complex on graphite in abiotic systems

Cyclic voltammetry was used to characterize the electrochemical activity of the PB modified graphite cathode. Fig. 3a shows the scan rate dependent cyclic voltammetry behavior of PB with the typical characteristics of their redox peak pairs and agrees with reported results [33]. A redox peak center located at 0.42 V is due to the electrochemical transformation of PB to Prussian white (PW), while a redox peak at 1.07 V corresponds to the transformation of PG (Prussian green) to PB. The related electrochemical reaction occurs due to an electron transfer between the Fe(II) and Fe(III) site of the complex as shown below (eqn. 1, 2) [33,34].

$$KFe^{III}[Fe^{II}(CN)_6] + e^- + K^+ \leftrightarrow K_2Fe^{II}[Fe^{II}(CN)_6] \quad .....(1) \quad E^0 = 0.42\ V$$

PB PW

$$KFe^{III}[Fe^{III}(CN)_6] \leftrightarrow KFe^{III}[Fe^{II}(CN)_6] + e^- \quad ..... (2) \quad E^0 = 1.07\ V$$

PG PB

The anodic and cathodic peak current ratio (I_c/I_a) of each of the redox peak potentials centered at 0.42 V and 1.07 V were 1.15 ± 0.02 and 1.01 ± 0.01, respectively. A value close to 1 indicates that the PB modified electrodes demonstrate an electrochemical redox reaction that is reversible at the graphite electrode surface [34]. Also, the peak potential differences (ΔE) of each redox pair was in the range of 87 mV to 142 mV, which is in agreement with previous studies [35]. The plot (data not shown) of peak current (anodic and cathodic) linearly increased with the square root of the scan rate (0.997 correlation coefficient). This indicates that the electrochemical process is controlled by diffusion. The reversibility of PB (ferric polynuclear complex) and PW (ferrous polynuclear complex) is an important characteristic for using these chemicals as redox mediators for TIE-1. Because many biological surfaces exhibit only slow heterogeneous electron transfer at the solid electrode surfaces, redox mediators (e.g., Prussian blue, Neutral red, Thionine, methylene blue, etc.) are used to facilitate the electron transfer between biological surfaces (e.g., microorganisms) and abiotic electrode surfaces [36-39]. These redox mediators can be electrochemically regenerated to transfer electrons to microorganisms. At the potential <0.4 V, Prussian blue ($K_2Fe^{II/III}[Fe^{II}(CN)_6]$) shows reversibility of the ferrous–ferric state in the outer iron complex. The reduced form of Prussian white (PW), ($K_2Fe^{II}[Fe^{II}(CN)_6]$) consists of the ferrous state in the outer iron complex, which can donate electrons to microorganisms. The poised electrodes can then regenerate the outer ferric ion complex by cathodic reduction. The electrochemical deposition strategy of the Prussian blue (PB) complex is well characterized in biosensor applications [40-42]. In addition, here we characterized the deposited PB on graphite using surface analytical techniques such as Scanning Electron Microscopy (SEM), X-Ray Photon Spectroscopy (XPS), EDS, and thickness measurements using SEM and a profilometer.

"Here Fig. 3"

The electrochemically deposited PB complex was further studied using surface analytical techniques such as SEM and XPS (Fig. 3b and Fig. 3c, d). The structure of the PB matrix and elemental composition could potentially influence biofilm formation and microbial electroactivity. Fig. 3b shows the SEM of PB deposited on graphite. We saw that PB was deposited as nanoparticles with a size of 70-130 nm and formed a layer (thickness of 670-729 nm). These PB nanoparticles can maximize the contact of microbes with the graphite surface. Further, to confirm the elemental composition of the electrodeposited PB, XPS analysis was performed. Fig. 3c shows the full range XPS spectrum of the PB complex, which consists of main peaks such as N 1s, C 1s and Fe 2p that can be clearly seen.

Also, deconvoluted XPS spectra for Fe 2p (Fig. 3d) indicate the oxidation states of Fe in the PB complex. We observe that Fe 2p is composed of two groups of peaks namely, Fe $2p_{3/2}$ (at a lower binding energy) and Fe $2p_{1/2}$ (at higher binding energy).
The peaks at 708.8 eV ($Fe2p_{3/2}$) and 721.7 eV ($Fe2p_{1/2}$) can be correlated to the presence of Fe(II). The peaks at 713.1 eV ($Fe2p_{3/2}$) and 723.7 eV ($Fe2p_{1/2}$) can be assigned to Fe(III). Based on the results obtained from XPS, the electrodeposited complex can be assigned as insoluble PB complex with a formula of PB as $Fe_4^{III}[Fe^{II}(CN)_6]_3$ [43-45].

3.3. Cathodic current uptake by TIE-1 from PB modified electrodes

The redox reversibility of the PB complex modified electrode was confirmed with CV analysis prior to use in bioelectrochemical studies (Fig. 4a). After inoculating TIE-1 in the bioreactor, the cathodic current was measured with unmodified graphite (GR-TIE-1), graphite with chitosan (GR/Chit-TIE-1), and graphite with PB/chitosan (GR-PB/Chit-TIE-1) electrode (Fig. 4). In all cases, the "no cell" control reactor did not show any significant current uptake over the operation period. However, TIE-1 inoculated systems showed the ability of cathodic current uptake within 24 h in all biocathodes. The maximum cathodic current (I_{max}) uptake by TIE-1 was 5.6 ± 0.09 μA/cm^2 (GR/PB/Chit-TIE-1) > 1.61 ± 0.15 μA/cm^2 (GR/Chit-TIE-1) > 1.47 ± 0.04 μA/cm^2 (GR-TIE-1). This indicates that the chitosan-modification alone only slightly improved current consumption compared with unmodified graphite. However, the PB modified electrode significantly enhanced the electron uptake by TIE-1 (up to 3.8 times). This effect was comparable with the cathodic electron uptake by *E. coli* using cathodes modified with cytocompatible electron mediators composed of redox polymers (7.8 μA/cm^2) [46]. The total quantity of current consumption (Fig. 4d-e) was assessed as -1.74 ± 0.03 mA h (for GR/PB/Chit-TIE-1), which is ~3.2 times higher than the unmodified (-0.53 ± 0.01 mA h) and the chitosan modified graphite cathode (-0.61 ± 0.05 mA h). The observed planktonic OD_{660} supports this trend; 0.023 (GR/PB/Chit-TIE-1), 0.014 (GR/Chit-TIE-1), and 0.014 (GR-TIE-1). Based on the molecular formula of cell biomass ($CH_{2.08}O_{0.53}N_{0.24}$, molecular weight of 26 g/mol), 1 C-mole of biomass is equivalent to 4 mole of electrons [47-49]. It was reported that total electron moles captured in cell biomass can be calculated (e.g., model anaerobic acetogenic bacterium *Moorella thermoacetica* culture, 1 OD equivalent to ~0.46 g dry cell weight/L) in terms of OD. The relationship between electron uptake and biomass in terms of OD were reported as (4.3 mol e^- x OD x 4.6 g dry cell L^{-1}) /26 g mol^{-1} [47]. Using this formula, in our system the total mole electrons captured by cell biomass in terms of observed OD will be 0.175 mol e^- (GR/PB/Chit-TIE-1), 0.0107 mol e^- (GR/Chit-TIE-1), and 0.0107 mol e^- (GR-TIE-1).

"Here Fig. 4"

CV and DPV were performed to characterize the bioelectrochemical redox activity of TIE-1. Fig. 5a-c shows the CV of modified and unmodified biocathodes compared with sterile cathodes at a scan rate of 5 mV/s. The midpoint redox potentials (E_p' and E_p") of GR-TIE-1, GR/Chit-TIE-1 or GR/PB/Chit-TIE-1 (Fig. 5a-c) are 0.187 V (E_p'), and 0.295 V (E_p"), which is closely related to the midpoint redox potential reported previously for TIE-1 [21]. Interestingly, the PB complex modified biocathode (Fig. 5c) retains the two

midpoint redox potentials of TIE-1 at 0.187 V and 0.295 V. The improved redox current was observed at 0.295 V due to the reversibility of PB (Fig. 5c). Although CV is an essential characterization technique to detect redox reactions that occur at the electrode surface, it has a low detection limit [50-52]. Pulse voltammetry techniques have frequently been used as complementary methods to CV. For pulse voltammetry techniques, the charging current can be lowered, and this lends higher sensitivity to our ability to measure Faradaic current at the redox signal [53,54]. Differential peak current (ΔI) at the redox signal (background current subtracted signal**)** was derived from the differential pulse voltammogram (Fig. 5d-f) to measure the biofilm's electroactivity. In all biocathodes, DPV consistently exhibits redox signals (E_p' and E_p") with the redox potential of 0.187 V and 0.295 V as seen in the CV results. Also, the redox signal (E_p) at 0.295 V shows the peak differential current (ΔI) of 88.4 μA/cm^2 for the GR/PB/Chit-TIE cathode (Fig. 5f). This is 7.6 times higher than the unmodified biocathode (11.4 μA/cm^2, GR-TIE-1), and is 5.9 times higher than chitosan modified biocathode (14.8 μA/cm^2, GR/Chit-TIE-1).

"Here Fig. 5"

Further, the DPV results support that the PB complex acts as an immobilized electron transfer mediator for TIE-1. The redox peak current is directly proportional to the concentration of electrochemically active molecules at the surface of the cathode. The surface covered electroactive sites in the biocathodes were calculated from the CV results by integrating charge under either the anodic or cathodic peaks. The surface coverage of electroactive moieties per unit area of the biocathode was 2.360 x 10^{-10} mol/cm^2 for GR/PB/Chit-TIE-1, 3.0624 x 10^{-11} mol/cm^2 for GR/Chit-TIE-1 and 1.7923 x 10^{-11} mol/cm^2 for GR-TIE-1 respectively [55,56]. Based on the surface coverage value, the PB complex modified biocathode promotes the electroactivity of the biofilm by one order of magnitude compared to the unmodified and chitosan modified biocathodes per unit area. It should be further noted that chitosan has positively charged terminal groups, which may help enhance the surface functionality by attracting bacteria, and providing a microenvironment for biological reactions at the biocathode [53,57,58]. The biocathodes were scanned from 0.1 V to 0.6 V at different sweep rates from 1 to 5 mV/s in a cell-free medium solution (Fig. 6a-c). This CV study (Fig. 6a-c) is to confirm that the redox activity of the biocathode is due to surface-attached redox molecules and not from the medium or electrolyte. In order to measure the redox activity of the biocathode with attached TIE- and not the plankton, the spent medium and the plankton was replaced with fresh cell-free medium to perform CVs. We observed that the mid-point potential of all biocathodes with attached TIE-1 retained their midpoint redox potentials as seen in the previous CVs of the bioreactors. A slight redox potential shift (15-20 mV) was observable perhaps due to the addition of fresh medium. The biocathode peak currents (anodic or cathodic) increased linearly with an increase in sweep rate (Fig. 6d). The linear correlation (R^2= 0.999) of peak currents with the sweep rate indicates that the biocathode used a surface or diffusion controlled bioelectrochemical reaction [56,59]. This might be due to the effect of the electron transfer mediator at the bio-interface. Further, the spent medium (cells free) of all reactors were analyzed for any dissolved redox ions (e.g., PB complex) or any self-excreted redox component from TIE-1 using voltammetry techniques such as CV (Fig. 6e) and DPV (Fig. 6f) with glassy carbon as working electrode [22]. The results reveal that no obvious redox

peaks exist in the potential region of 0.2 to 0.3 V in the spent medium. This confirms that the PB complex modified biocathode does not shed PB during the experiments, and that PB is surface confined when covered by a chitosan layer.

"Here Fig. 6"

EIS characterization of the biocathodes was performed at the end of the EU experiment as shown in Fig. 7a. The EIS data were fitted into the equivalent circuit of R(Q(R(Q(RW)))) to derive the value of the circuit component [56,60]. The equivalent circuit consists of resistance offered by solution (R_s), constant phase element of Helmholtz and biofilm layer (Q), parallel to their respective charge transfer resistance across the Helmholtz layer (R_{ct}), and the biofilm layer ($R_{biofilm}$) followed by Warburg's diffusion element (W) and is shown as an inset in Fig. 7a. The values of the circuit components are listed in Table S2. When the cathode interacts with microbes (biofilm), the $R_{biofilm}$ value decreases gradually. The lower value of $R_{biofilm}$ implies a faster bioelectrochemical reaction. Based on the simulated equivalent circuit, the $R_{biofilm}$ value of the biocathodes was found to be 5143 ± 9.2 Ω (GR-TIE-1) >141.1 ± 2.2 Ω (GR/Chit-TIE-1) > 13.3 ± 2.8 Ω (GR/PB/Chit-TIE-1). The lower $R_{biofilm}$ value might be due to the GR/PB/Chit-TIE-1 biocathode having an accelerated electrode reaction rate and higher current uptake as observed by CA and CV studies. Further, the lower $R_{biofilm}$ of the modified biocathodes (e.g., Chitosan or PB complex cathode) can be explained by the nature of the ionically conductive biopolymer chitosan, which will help the bacterial cells make electrochemical contact with the electrode. The cathodes modified with an electron transfer mediator (PB complex) will enhance electron donation to bacteria, further lowering the $R_{biofilm}$. Potentiodynamic polarization (Tafel plots) of biocathodes was performed to evaluate the bioelectrochemical kinetics of surface bound redox probe, or PB modified cathodes with TIE-1 (Fig. 7b-c and Table S3). It indicates that the exchange current of GR/PB/Chit-TIE-1 was 10.3 ± 0.07 µA, which is about ten times higher than the unmodified biocathode (1.05 ± 0.02 µA, GR/TIE-1), and five times higher than the chitosan-based biocathode (1.9 ± 0.02 µA). The value of exchange current (I_0) supports the current uptake trends observed in the EU and CV experiments. The biocathode potential at the intersection of the anodic and cathodic region for GR/PB/Chit-TIE-1 has a higher cathodic value (+45 mV) compared with the other biocathodes. The lower value of the anodic (β_a = 62.3 mV/dec) and cathodic (β_c = 197.2 mV/dec) slope can be attributed to the enhanced reaction rate of extracellular electron transfer at the biointerface of the GR/PB/Chit-TIE-1 biocathode.

Based on electrochemical analysis, the enhanced performance of PB based biocathodes is due to the reversible redox reaction between PB (Ferric polynuclear complex) and PW (Ferrous polynuclear complex). At the cathodic reduction potential of +100 mV, the electrode surface bound with the PW is able to donate electrons continuously to TIE-1. Further, the microbially oxidized PB is cyclically reduced to PW by the poised potential enhancing extracellular electron transfer to TIE-1, and biomass production from CO_2 (Fig. S1). From SEM images, it is evident that the attachment ability of TIE-1 clearly improved on the modified graphite cathode compared to the unmodified electrode (Fig. S5). Further, both modified cathodes consist of a network of chitosan, which appears to aid microbial attachment as supported by the higher current density utilized by TIE-1. The

chitosan (biopolymer) is used to enhance the microbial attachment that we clearly see from SEM images of GR/Chit/TIE-1 (Fig. S5c). However, the electron uptake with and without chitosan shows similar values, which is likely due to the lack of redox active or mediator molecules in the chitosan. Although more cells attach to the GR/Chit-TIE-1 electrodes, because chitosan is not electrochemically active, improved attachment of cells to chitosan does not lead to higher electron uptake. The GR/PB/TIE-1 (no chitosan) was avoided due to potential issues of detachment/dissolution of PB without chitosan. The chitosan network holds the PB layer and provides an immobilized surface for microbial attachment (Fig. S5d). The "with and without chitosan" controls clearly show that microbial uptake is unaffected by the presence or absence of chitosan, further supporting the fact that chitosan does not affect microbial electron uptake significantly.

"Here Fig. 7"

3.4. Implications on future MES studies

This work emphasizes that the PB modified graphite electrodes enhance electron uptake (cathodic reduction current) by 3.8 – fold with respect to current density (0.0568 ± 0.09 A/m^2) when compared to unmodified graphite. However, this electron uptake is not observed when we add Fe(II) to the system (Table 1). Further, the dissolved Fe(II) added to the medium is electrochemically and/or biologically oxidized to Ferrihydrite (oxides of Fe(III)) at the surface of the electrode as well as on the TIE-1 cell surface (Fig. 2, Fig. S2, Fig. S3 & Fig. S4). This oxidation was supported by lower anodic current with the biotic system ($FeCl_2$+TIE-1, 17.61 ± 1.3 $\mu A/cm^2$) than with the abiotic system ($FeCl_2$, 21.18 ± 2.2 $\mu A/cm^2$) from Table 1. This lower anodic current in the biotic system ($FeCl_2$+TIE-1) can be the effect of lower electrochemical oxidation of Fe(II). Biotic reactors with Fe(II) showed anodic current in contrast to those coated with PB-Chitosan (GR/PB/Chit-TIE-1) that showed higher cathodic current than unmodified graphite electrodes (GR/TIE-1).

"Here Table 1"

Recently many researchers have explored the importance of direct electron uptake and utilization of electrons from various biocathodes in MESs for biofuel production [3,61,62]. MESs mimic the process of natural autotrophy by using carbon dioxide as a carbon source for biosynthesis [62]. In MES applications, a surplus amount of electron uptake is required to reduce carbon dioxide to biofuels/biochemical in contrast to the utilization of already reduced carbon sources as feedstocks (eg., sugars, glycerol) [62]. Our modified biocathode with TIE-1 (GR/PB/Chit-TIE-1) showed a reproducible increase in electron uptake (*3.2- fold* higher for current consumption, -0.593 ± 06 mA h to -1.74 ± 0.03 mA h, and *3.8-fold* higher current density 1.47 ± 0.04 to 5.6 ± 0.09 $\mu A/cm^2$). This effect can play a significant role in direct electron transfer strategies (biocathode poised at which no H_2 production) in the field of MES [63]. For context, in a recent study authors showed that changing the electrode material to graphite felt and increasing the time of operation of a BEC with *Clostridium pasteurianum* increased both current density (-1.5 ~ -5 mA or -14 $\mu A/cm^2$ ~ -46 $\mu A/cm^2$, *3-fold* increase) and biobutanol production from glucose +45 mV vs. SHE (*6-fold* increase) [62]. This improvement in current density is in the range of what we report here for direct electron uptake by TIE-1 using a PB modified electrode. The

increase in current density also led to increased biomass (*2-fold* higher) which is the first step toward improving bioproduction using TIE-1. This work also clarifies the influence of soluble and insoluble iron forms on electron uptake by TIE-1, paving the way for understanding the mechanisms underlying electron uptake. Such mechanistic insight is also crucial for future MES application. Future work will explore the use of natural iron oxides coated electrodes as potential redox mediators for TIE-1.

4. Conclusions

In summary, electrodes modified with the redox complex Prussian blue (PB) improved electron transfer to the photoelectroautotroph, *Rhodopseudomonas palustris* TIE-1. The PB complex based biocathode showed increased cathodic current density (5.6 ± 0.09 μA/cm^2), which is 3.8 times higher than the unmodified biocathode. A higher current uptake capacity (-1.744 ± 0.03 mA h for 130 h), and lower charge transfer resistance of the PB based biocathode ($R_{biofilm}$, 20.6 ± 2.8 Ω) suggests that the reversible redox nature of the PB complex acts as an electron transfer (ET) agent. Our results indicate that the modified biocathode offers an advantage to TIE-1 grown under photoelectroautotrophic conditions by increasing electron transfer rates and current density. TIE-1 is a prime candidate for microbial electrosynthesis, and these modified electrodes will aid higher bio-production of value-added biochemicals.

Acknowledgements

The authors would like to acknowledge financial support from US Department of Energy (grant number DESC0014613) and the David and Lucile Packard Foundation to carry out this research. We also thank Mr. Michael Guzman, Washington University in Saint Louis, USA, and our anomymous reviewers for their valuable comments.

References

[1] K. Rabaey, P. Girguis, L.K. Nielsen, Metabolic and practical considerations on microbial electrosynthesis, Curr. Opin. Biotechnol. 22 (2011) 371-377.

[2] C.W. Marshall, D.E. Ross, E.B. Fichot, R.S. Norman, H.D. May, Long-term operation of microbial electrosynthesis systems improves acetate production by autotrophic microbiomes, Environ. Sci. Technol. 47 (2013) 6023-6029.

[3] H.D. May, P.J. Evans, E.V. LaBelle, The bioelectrosynthesis of acetate, Curr. Opin. Biotechnol. 42 (2016) 225-233.

[4] S. Bajracharya, S. Srikanth, G. Mohanakrishna, R. Zacharia, D.P. Strik, D. Pant, Biotransformation of carbon dioxide in bioelectrochemical systems: State of the art and future prospects, J. Power Sources, 356 (2017) 256-273.

[5] C.W. Marshall, D.E. Ross, E.B. Fichot, R.S. Norman, H.D. May, Electrosynthesis of commodity chemicals by an autotrophic microbial community, Appl. Environ. Microbiol. 78 (2012) 8412-8420.

[6] M. Siegert, M.D. Yates, A.M. Spormann, B.E. Logan, Methanobacterium dominates biocathodic archaeal communities in methanogenic microbial electrolysis cells, ACS Sus. Chem. Eng. 3 (2015) 1668-1676.

[7] G. Mohanakrishna, K. Vanbroekhoven, D. Pant, Imperative role of applied potential and inorganic carbon source on acetate production through microbial electrosynthesis, J. CO_2 Util. 5 (2016) 57-64.

[8] F. Kracke, B. Virdis, P.V. Bernhardt, K. Rabaey, J.O. Kromer, Redox dependent metabolic shift in *Clostridium autoethanogenum* by extracellular electron supply, Biotechnol. Biofuels 9 (2016) 249.

[9] C.S. Butler, D.R. Lovley, How to Sustainably Feed a Microbe: Strategies for biological production of carbon-based commodities with renewable electricity, Front. Microbiol. 7 (2016) 1879.

[10] P.L. Tremblay, T. Zhang, Electrifying microbes for the production of chemicals, Front. Microbiol. 6 (2015) 201.

[11] P.L. Tremblay, L.T. Angenent, T. Zhang, Extracellular electron uptake: among autotrophs and mediated by surfaces, Trends Biotechnol. 35 (2017) 360-371.

[12] S. Bajracharya, R. Yuliasni, K. Vanbroekhoven, C.J.N. Buisman, D. Strik, D. Pant, Long-term operation of microbial electrosynthesis cell reducing CO_2 to multi-carbon chemicals with a mixed culture avoiding methanogenesis, Bioelectrochem. 113 (2017) 26-34.

[13] M. Villano, F. Aulenta, C. Ciucci, T. Ferri, A. Giuliano, M. Majone, Bioelectrochemical reduction of CO_2 to CH_4 via direct and indirect extracellular electron transfer by a hydrogenophilic methanogenic culture, Bioresour. Technol. 101 (2010) 3085-3090.

[14] E. Blanchet, F. Duquenne, Y. Rafrafi, L. Etcheverry, B. Erable, A. Bergel, Importance of the hydrogen route in up-scaling electrosynthesis for microbial CO_2 reduction, Energ. Environmen. Sci. 8 (2015) 3731-3744.

[15] H. Li, P.H. Opgenorth, D.G. Wernick, S. Rogers, T.Y. Wu, W. Higashide, P. Malati, Y.X. Huo, K.M. Cho, J.C. Liao, Integrated electromicrobial conversion of CO_2 to higher alcohols, Science 335 (2012) 1596-1596.

[16] S.A. Cheng, D.F. Xing, D.F. Call, B.E. Logan, Direct biological conversion of electrical current into methane by electromethanogenesis, Environ. Sci. Technol. 43 (2009) 3953-3958.

[17] K.P. Nevin, T.L. Woodard, A.E. Franks, Z.M. Summers, D.R. Lovley, Microbial electrosynthesis: feeding microbes electricity to convert carbon dioxide and water to multicarbon extracellular organic compounds, Mbio 1 (2010).

[18] P.F. Beese-Vasbender, J.P. Grote, J. Garrelfs, M. Stratmann, K.J.J. Mayrhofer, Selective microbial electrosynthesis of methane by a pure culture of a marine lithoautotrophic archaeon, Bioelectrochemistry 102 (2015) 50-55.

[19] P. Batlle-Vilanova, S. Puig, R. Gonzalez-Olmos, M.D. Balaguer, J. Colprim, Continuous acetate production through microbial electrosynthesis from CO_2 with microbial mixed culture, J. chem. Technol. Biotechnol. 91 (2016) 921-927.

[20] Y. Jiao, D.K. Newman, The *pio* operon is essential for phototrophic Fe(II) oxidation in *Rhodopseudomonas palustris* TIE-1, J. Bacteriol. 189 (2007) 1765-1773.

[21] A. Bose, D.K. Newman, Regulation of the phototrophic iron oxidation (*pio*) genes in *Rhodopseudomonas palustris* TIE-1 is mediated by the global regulator, FixK, Mol. Microbiol. 79 (2011) 63-75.

[22] A. Bose, E.J. Gardel, C. Vidoudez, E.A. Parra, P.R. Girguis, Electron uptake by iron-oxidizing phototrophic bacteria, Nature Commun. 5 (2014).

[23] D.F.R. Doud, L.T. Angenent, Toward electrosynthesis with uncoupled extracellular electron uptake and metabolic growth: enhancing current uptake with *Rhodopseudomonas palustris*, Environ. Sci. Technol. Lett. 1 (2014) 351-355.

[24] L.J. Bird, V. Bonnefoy, D.K. Newman, Bioenergetic challenges of microbial iron metabolisms, Trends Microbiol. 19 (2011) 330-340.

[25] D.H. Park, J.G. Zeikus, Utilization of electrically reduced neutral red by *Actinobacillus succinogenes*: physiological function of neutral red in membrane-driven fumarate reduction and energy conservation, J. Bacteriol. 181 (1999) 2403-2410.

[26] O. Choi, B.I. Sang, Extracellular electron transfer from cathode to microbes: application for biofuel production, Biotechnol. Biofuels 9 (2016).

[27] Gaviglio, F. Battaglini, Hydrogen peroxide detection under physiological conditions by Prussian blue stabilized using a polyelectrolyte-surfactant complex matrix, Sens. Act. B-Chem. 182 (2013) 53-57.

[28] F. Ricci, G. Palleschi, Sensor and biosensor preparation, optimisation and applications of Prussian Blue modified electrodes, Biosens. Bioelectron. 21 (2005) 389-407.

[29] X. Xie, M. Ye, C. Liu, P.C. Hsu, C.S. Criddle, Y. Cui, Use of low cost and easily regenerated Prussian Blue cathodes for efficient electrical energy recovery in a microbial battery, Energ. Environ. Sci. 8 (2015) 546-551.

[30] J. Zhao, P. Yue, S. Tricard, T. Pang, Y. Yang, J. Fang, Prussian blue (PB)/carbon nanopolyhedra/polypyrrole composite as electrode: a high performance sensor to detect hydrazine with long linear range, Sens. Act. B: Chem. 251 (2017) 706-712.

[31] A. Ehrenreich, F. Widdel, Anaerobic oxidation of ferrous iron by purple bacteria, a new-type of phototrophic metabolism, Appl. Environ. Microbiol. 60 (1994) 4517-4526.

[32] J.J. Garcia-Jareno, D. Benito, J. Navarro-Laboulais, F. Vicente, Electrochemical behavior of electrodeposited prussian blue films on ITO electrode: an attractive laboratory experience, J. Chem. Edu. 75 (1998) 881.

[33] L.M.N. Assis, L. Ponez, A. Januszko, K. Grudzinski, A. Pawlicka, A green-yellow reflective electrochromic device, Electrochim. Acta 111 (2013) 299-304.

[34] Y. Ding, G. Gu, X.H. Xia, Electrochemical deposition and mechanism investigation of Prussian blue on graphic carbon paste electrode from an acidic ferricyanide solution, J. Solid State Electrochem. 12 (2008) 553-558.

[35] T. Tatsuma, Y. Kuroiwa, K. Ishii, K. Kudo, A. Sakoda, Uptake and electrochemical ejection of cesium ion by a prussian blue-modified electrode, Chem. Lett. 43 (2014) 1281-1283.

[36] S.D. Roller, H.P. Bennetto, G.M. Delaney, J.R. Mason, J.L. Stirling, C.F. Thurston, Electron-transfer coupling in microbial fuel cells: 1. comparison of redox-mediator reduction rates and respiratory rates of bacteria, J. Chem. Technol. Biotechnol. 34 (1984) 3-12

[37] A.K. Shukla, P. Suresh, S. Berchmans, A. Rajendran, Biological fuel cells and their applications, Curr. Sci. 87 (2004) 455-468.

[38] R.N. Krishnaraj, R. Karthikeyan, S. Berchmans, S. Chandran, P. Pal, Functionalization of electrochemically deposited chitosan films with alginate and prussian blue for enhanced performance of microbial fuel cells, Electrochim. Acta, 112 (2013) 465-472.

[39] O. Adelaja, T. Keshavarz, G. Kyazze, The effect of salinity, redox mediators and temperature on anaerobic biodegradation of petroleum hydrocarbons in microbial fuel cells, J. Hazard. Mater. 283 (2015) 211-217.

[40] D.T. Gimenes, E. Nossol, Effect of light source and applied potential in the electrochemical synthesis of Prussian blue on carbon nanotubes, Electrochim. Acta (2017). https://doi.org/10.1016/j.electacta.2017.08.142

[41] X. Zhai, Y. Li, J. Li, C. Yue, X. Lei, Electrochemical sensor for detection of hydrogen peroxide modified with prussian blue electrodeposition on nitrogen, phosphorus and sulfur co-doped porous carbons-chitosan, Mater. Sci. Eng. C 77 (2017) 1242-1246.

[42] X.-X. Dong, J.-Y. Yang, L. Luo, Y.-F. Zhang, C. Mao, Y.-M. Sun, H.-T. Lei, Y.-D. Shen, R.C. Beier, Z.-L. Xu, Portable amperometric immunosensor for histamine detection using Prussian blue-chitosan-gold nanoparticle nanocomposite films, Biosens. Bioelectron. 98 (2017) 305-309.

[43] A. Forment-Aliaga, R.T. Weitz, A.S. Sagar, E.J.H. Lee, M. Konuma, M. Burghard, K. Kern, Strong p-type doping of individual carbon nanotubes by prussian blue functionalization, Small 4 (2008) 1671-1675.

[44] Q. Sheng, R. Liu, J. Zheng, Prussian blue nanospheres synthesized in deep eutectic solvents, Nanoscale 4 (2012) 6880-6886.

[45] J. Marwan, T. Addou, D. Bélanger, Functionalization of glassy carbon electrodes with metal-based species, Chem. Mater. 17 (2005) 2395-2403.

[46] M. Kaneko, M. Ishikawa, J. Song, S. Kato, K. Hashimoto, S. Nakanishi, Cathodic supply of electrons to living microbial cells via cytocompatible redox-active polymers, Electrochem. Commun. 75 (2017) 17-20.

[47] S. Bajracharya, K. Vanbroekhoven, C.J.N. Buisman, D. Pant, D. Strik, Application of gas diffusion biocathode in microbial electrosynthesis from carbon dioxide, Environ. Sci. Pollut. Res. 23 (2016) 22292-22308.

[48] A.G. Fast, E.T. Papoutsakis, Stoichiometric and energetic analyses of non-photosynthetic CO_2-fixation pathways to support synthetic biology strategies for production of fuels and chemicals, Curr. Opin. Chem. Eng. 1 (2012).

[49] B.P. Tracy, S.W. Jones, A.G. Fast, D.C. Indurthi, E.T. Papoutsakis, Clostridia: the importance of their exceptional substrate and metabolite diversity for biofuel and biorefinery applications, Curr. Opin. Biotechnol. 23 (2012) 364-381.

[50] E. Marsili, J.B. Rollefson, D.B. Baron, R.M. Hozalski, D.R. Bond, Microbial biofilm voltammetry: direct electrochemical characterization of catalytic electrode-attached biofilms, Appl. Environ. Microbiol. 74 (2008) 7329-7337.

[51] Okamoto, K. Hashimoto, K.H. Nealson, R. Nakamura, Rate enhancement of bacterial extracellular electron transport involves bound flavin semiquinones, Proc. Nat. Acad. Sci. U.S.A 110 (2013) 7856-7861.

[52] M. Sharma, P. Jain, J.L. Varanasi, B. Lal, J. Rodriguez, J.M. Lema, P.M. Sarma, Enhanced performance of sulfate reducing bacteria based biocathode using stainless steel mesh on activated carbon fabric electrode, Bioresour. Technol. 150 (2013) 172-180.

[53] H.H. Liu, J.L. Lu, M. Zhang, D.W. Pang, H.D. Abruna, Direct electrochemistry of cytochrome c surface-confined on DNA-modified gold electrodes, J. Electroanal. Chem. 544 (2003) 93-100.

[54] Kashyap, P.K. Dwivedi, J.K. Pandey, Y.H. Kim, G.M. Kim, A. Sharma, S. Goel, Application of electrochemical impedance spectroscopy in bio-fuel cell characterization: a review, Int. J. Hydrog. Energ. 39 (2014) 20159-20170.

[55] Y. Yuan, S.G. Zhou, N. Xu, L. Zhuang, Electrochemical characterization of anodic biofilms enriched with glucose and acetate in single-chamber microbial fuel cells, Colloids Surf. B-Biointerfaces 82 (2011) 641-646.

[56] R. Karthikeyan, B. Wang, J. Xuan, J.W.C. Wong, P.K.H. Lee, M.K.H. Leung, Interfacial electron transfer and bioelectrocatalysis of carbonized plant material as effective anode of microbial fuel cell, Electrochim. Acta, 157 (2015) 314-323.

[57] S. El Ichi, A. Zebda, A. Laaroussi, N. Reverdy-Bruas, D. Chaussy, M.N. Belgacem, P. Cinquin, D.K. Martin, Chitosan improves stability of carbon nanotube biocathodes for glucose biofuel cells, Chem. Commun. 50 (2014) 14535-14538.

[58] S. El Ichi, A. Zebda, J.P. Alcaraz, A. Laaroussi, F. Boucher, J. Boutonnat, N. Reverdy-Bruas, D. Chaussy, M.N. Belgacem, P. Cinquin, D.K. Martin, Bioelectrodes modified with chitosan for long-term energy supply from the body, Energ. Environ. Sci. 8 (2015) 1017-1026.

[59] K.P. Gregoire, S.M. Glaven, J. Hervey, B.C. Lin, L.M. Tender, Enrichment of a high-current density denitrifying microbial biocathode, J. Electrochem. Soc. 161 (2014) H3049-H3057.

[60] J.T. Babauta, H. Beyenal, Mass transfer studies of *Geobacter sulfurreducens* biofilms on rotating disk electrodes, Biotechnol. Bioeng. 111 (2014) 285-294.

[61] A.S. Hawkins, Y. Han, H. Lian, A.J. Loder, A.L. Menon, I.J. Iwuchukwu, M. Keller, T.T. Leuko, M.W.W. Adams, R.M. Kelly, Extremely thermophilic routes to microbial electrofuels, ACS Catal. 1 (2011) 1043-1050.

[62] O. Choi, T. Kim, H.M. Woo, Y. Um, Electricity-driven metabolic shift through direct electron uptake by electroactive heterotroph *Clostridium pasteurianum*, Sci. Rep. 4 (2014).

[63] J.S. Deutzmann, M. Sahin, A.M. Spormann, Extracellular enzymes facilitate electron uptake in biocorrosion and bioelectrosynthesis, MBio 6 (2015).

Tables:

Table 1. Summary of anodic or cathodic current (n=3) with different systems at a poised potential of +100 mV vs. Standard Hydrogen Electrode

Systems	Total current (mA h)	Average peak current ($\mu A/cm^2$)
Control (no $FeCl_2$, no cell)	-0.0372 ± 008	-0.0887 ± 0.03
$FeCl_2$ (no cell)	3.498 ± 0.28	21.18 ± 2.2
$FeCl_2$ + TIE-1	2.594 ± 0.11	17.61 ± 1.3
GR-TIE-1	-0.593 ± 06	-1.47 ± 0.04
GR/Chit-TIE-1	-0.4859 ± 002	-1.61 ± 0.15
GR/PB/Chit-TIE-1	-1.7439 ± 002	-5.6 ± 0.09

Note: Positive values of current indicate anodic oxidation and Negative values of current indicate cathodic reduction or electron uptake

Figure captions:

Fig.1. Effect of $FeCl_2$ containing freshwater (FW) medium on Electron Uptake (EU) using unmodified graphite cathodes. Chronoamperometry (a); and the total current capacity (b) of abiotic (control), TIE-1 (biotic) followed by addition of $FeCl_2$ (TIE-1 → $FeCl_2$, biotic), $FeCl_2$(control) and $FeCl_2$ + TIE-1(biotic) on an unmodified graphite electrode at a poised potential of +100mV vs. Standard Hydrogen Electrode (SHE) for 152 h under N_2/CO_2. Standard deviation of replicated data (n=3) is shown. Cyclic voltammetry (5 mV/s) characteristics of added $FeCl_2$ in the abiotic (c); and biotic (d) system at the end of EU experiment.

Fig. 2. SEM images of graphite cathode at the end of the EU experiment with dissolved $FeCl_2$ in FW medium. (a, a') Biotic system ($FeCl_2$ + TIE-1) ; (b, b') Biotic system (TIE-1 → $FeCl_2$); and (c, c') abiotic system ($FeCl_2$). EDS (Electron Dispersive Spectroscopy) of square region is shown corresponding to the respective SEM images (a", b" and c").

Fig. 3. (a) Cyclic voltammetry of redox complex (PB) deposited graphite electrode in 0.1 M KCl at different scan rates; PB - Prussian blue, PW - Prussian white, PG - Prussian green; (b) SEM image of PB on graphite (insert: higher magnification image); (c) X-ray photoelectron spectroscopy (XPS) of PB complex; and (d) Fe 2p XPS of PB complex.

Fig. 4. Chronoamperometry of abiotic (control) and biotic (with TIE-1) graphite electrodes at poised potential of +100mV vs. SHE for 130 h under N_2/CO_2. Standard deviation of replicated data (n=3) were shown for Current density vs. Time (a, b, c); and Total current vs. Time (d, e, f).

Fig. 5. Representative cyclic voltammetry (a, b, c) of abiotic (control) graphite cathodes and biotic (with TIE-1) graphite electrodes were recorded in FW medium at a scan rate of 5 mV/s under N_2/CO_2; Differential Pulse Voltammetry (Potential vs. Differential current, ΔI) of biotic (with TIE-1) graphite electrodes (d, e, f).

Fig. 6. Scan rate dependence cyclic voltammetry of biotic (with TIE-1) graphite electrodes in 50 mM PBS (pH7); unmodified biocathode (a), biocathode modified with chitosan (b), biocathode modified with chitosan - Prussian blue (c). Linear relationship of anodic (solid symbols) and cathodic (open symbols) peak current with square root of scan rate, $\gamma^{1/2}$ (d). Cyclic Voltammetry (e) at a scan rate of 5 mV/s; and Differential Pulse Voltammetry (f) of cell-free spent medium (supernatant) at the end of EU experiment using a glassy carbon electrode.

Fig. 7 (a) Electrochemical impedance spectra (Real Impedance, Z' vs. Imaginary Impedance, Z") of graphite cathodes with a TIE-1 biofilm at a set potential of +100 mV vs SHE and Potentiodynamic (Tafel plot, logarithmic current vs. potential) polarization of graphite cathodes with TIE-1 biofilms; (b) Open circuit potential before polarization; (c) polarization of cathode from -250 mV to + 250 mV from open circuit potential.

Figures:

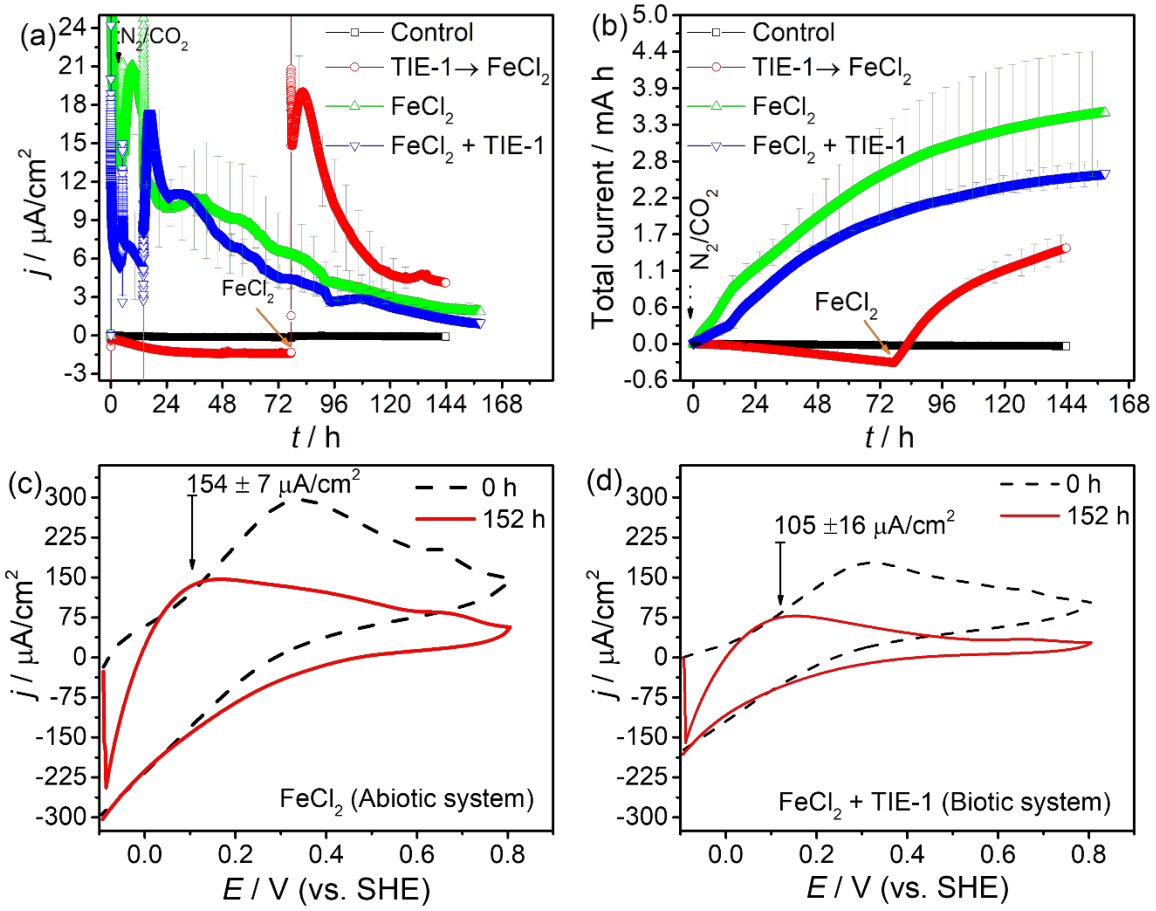

Fig. 1.

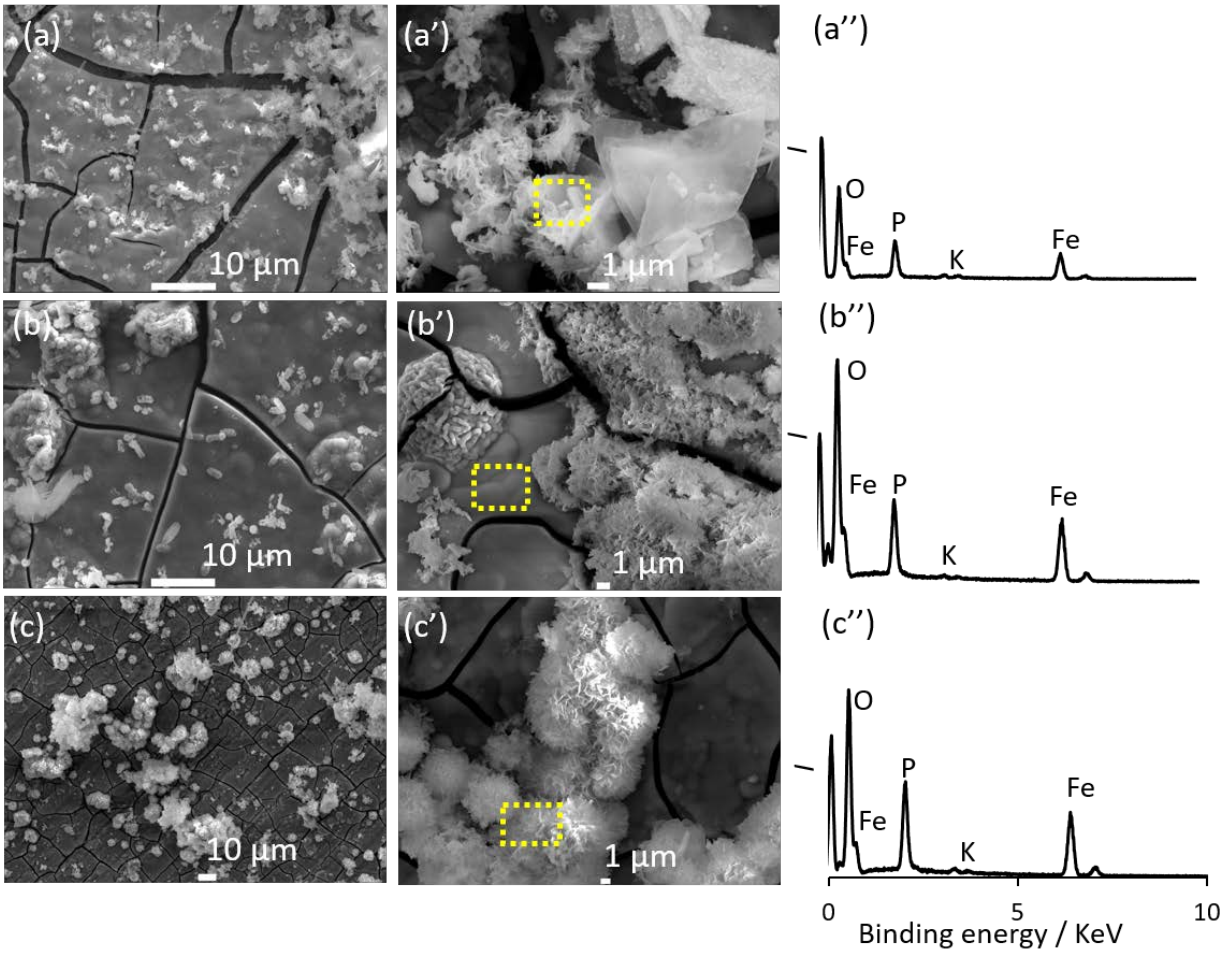
(a)
10 µm
(a')
1 µm
(a'')
O
Fe
P
K
Fe
(b)
10 µm
(b')
1 µm
(b'')
O
Fe
P
K
Fe
(c)
10 µm
(c')
1 µm
(c'')
O
Fe
P
K
Fe
0
5
10
Binding energy / KeV

Fig. 2.

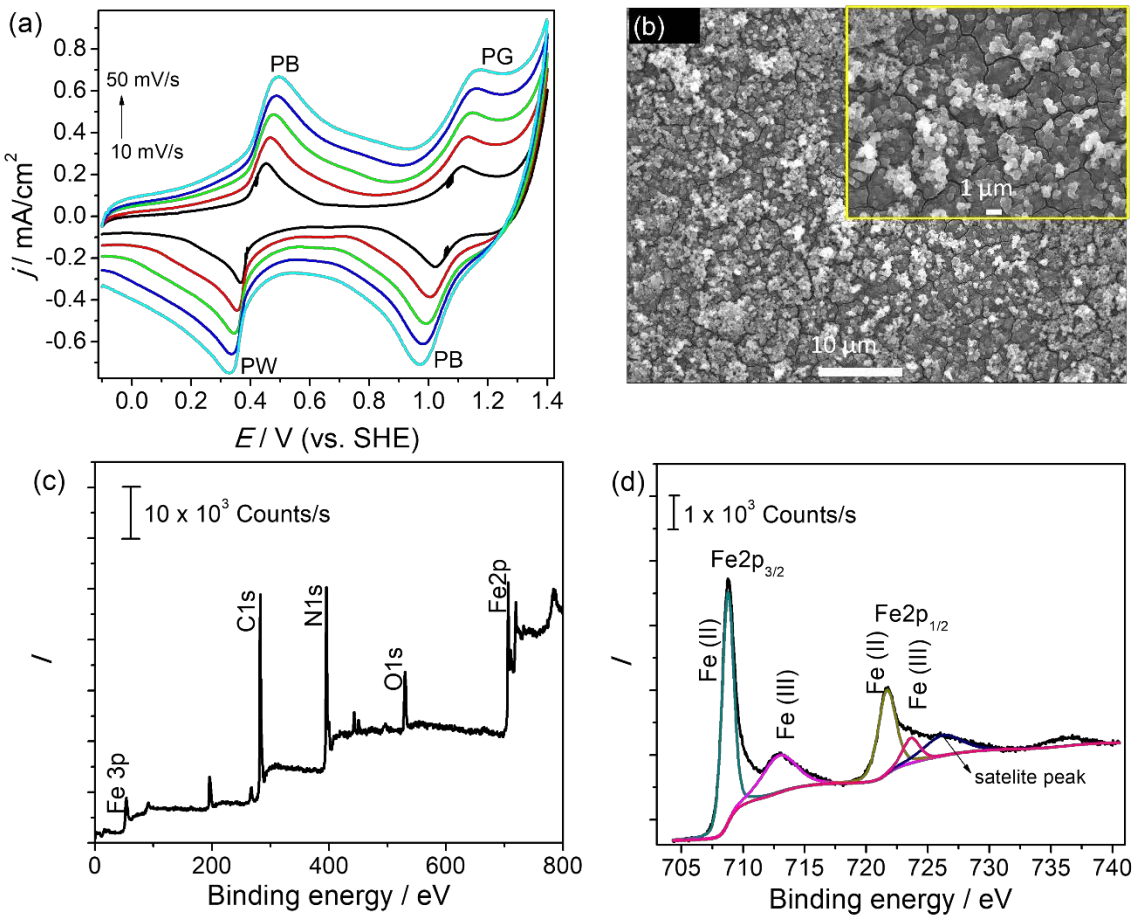
(a)
50 mV/s
10 mV/s
PB
PG
PW
PB
j / mA/cm2
E / V (vs. SHE)
(b)
1 µm
10 µm
(c)
10 x 10^3 Counts/s
Fe 3p
C1s
N1s
O1s
Fe2p
I
Binding energy / eV
(d)
1 x 10^3 Counts/s
Fe2p3/2
Fe2p1/2
Fe (II)
Fe (III)
Fe (II)
Fe (III)
satelite peak
I
Binding energy / eV

Fig. 3.

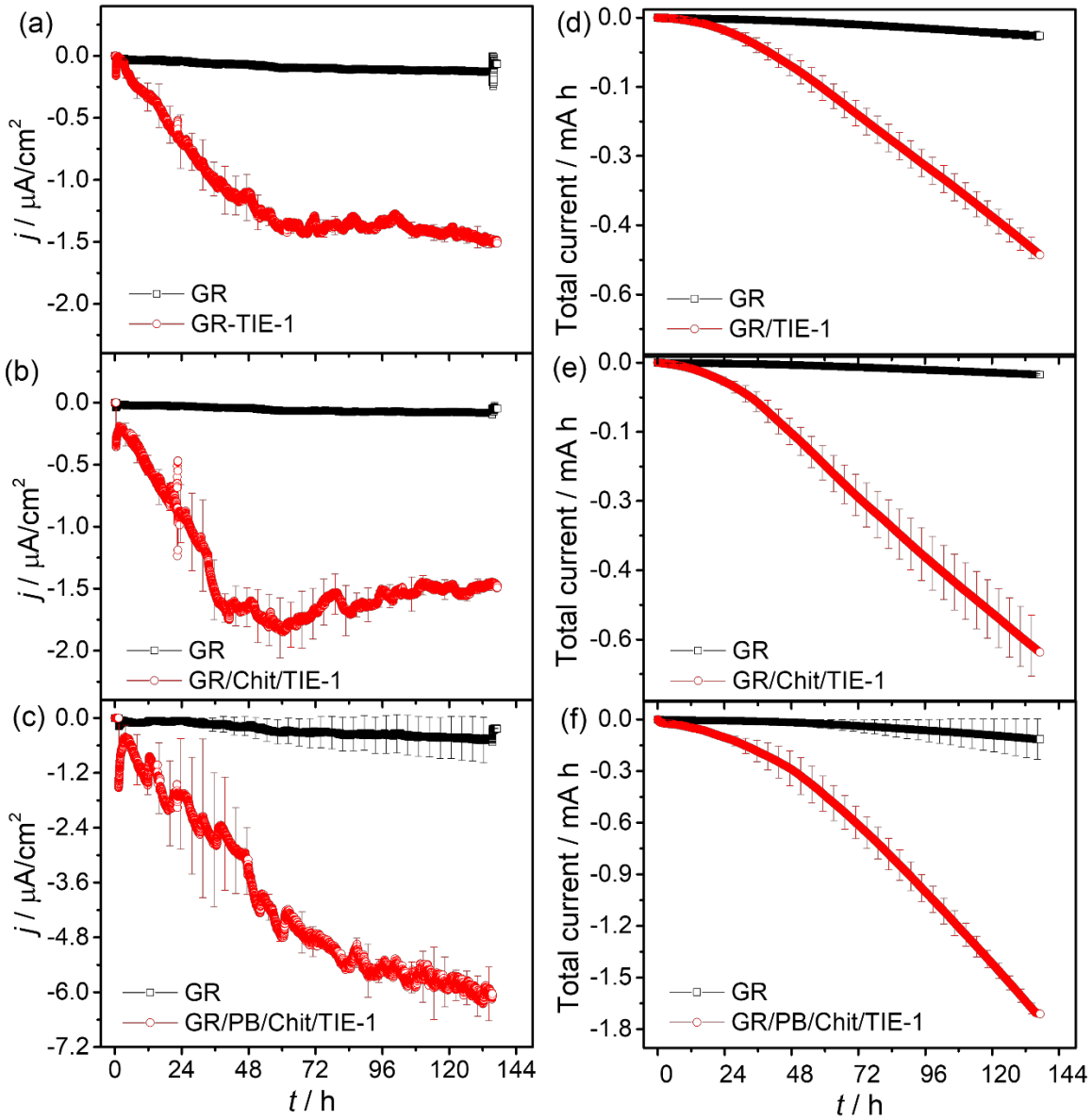
(a)
(b)
(c)
(d)
(e)
(f)
j / μA/cm²
Total current / mA h
t / h
GR
GR-TIE-1
GR/TIE-1
GR/Chit/TIE-1
GR/PB/Chit/TIE-1

Fig. 4.

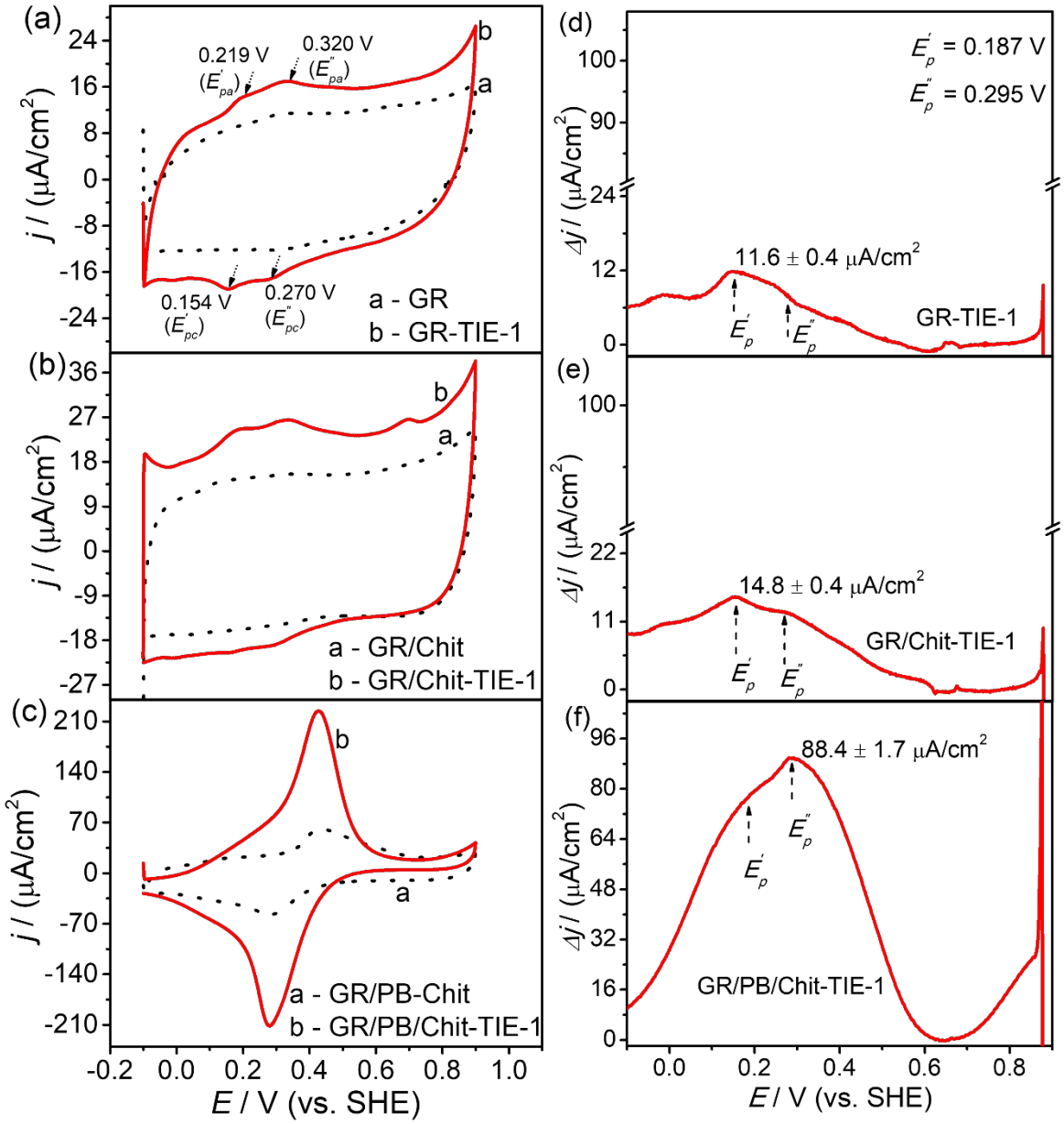
(a)
0.219 V
(E'_{pa})
0.320 V
(E''_{pa})
0.154 V
(E'_{pc})
0.270 V
(E''_{pc})
a - GR
b - GR-TIE-1
(b)
a - GR/Chit
b - GR/Chit-TIE-1
(c)
a - GR/PB-Chit
b - GR/PB/Chit-TIE-1
j / (μA/cm²)
E / V (vs. SHE)
(d)
E'_p = 0.187 V
E''_p = 0.295 V
11.6 ± 0.4 μA/cm²
GR-TIE-1
(e)
14.8 ± 0.4 μA/cm²
GR/Chit-TIE-1
(f)
88.4 ± 1.7 μA/cm²
GR/PB/Chit-TIE-1
Δj / (μA/cm²)
E / V (vs. SHE)

Fig. 5.

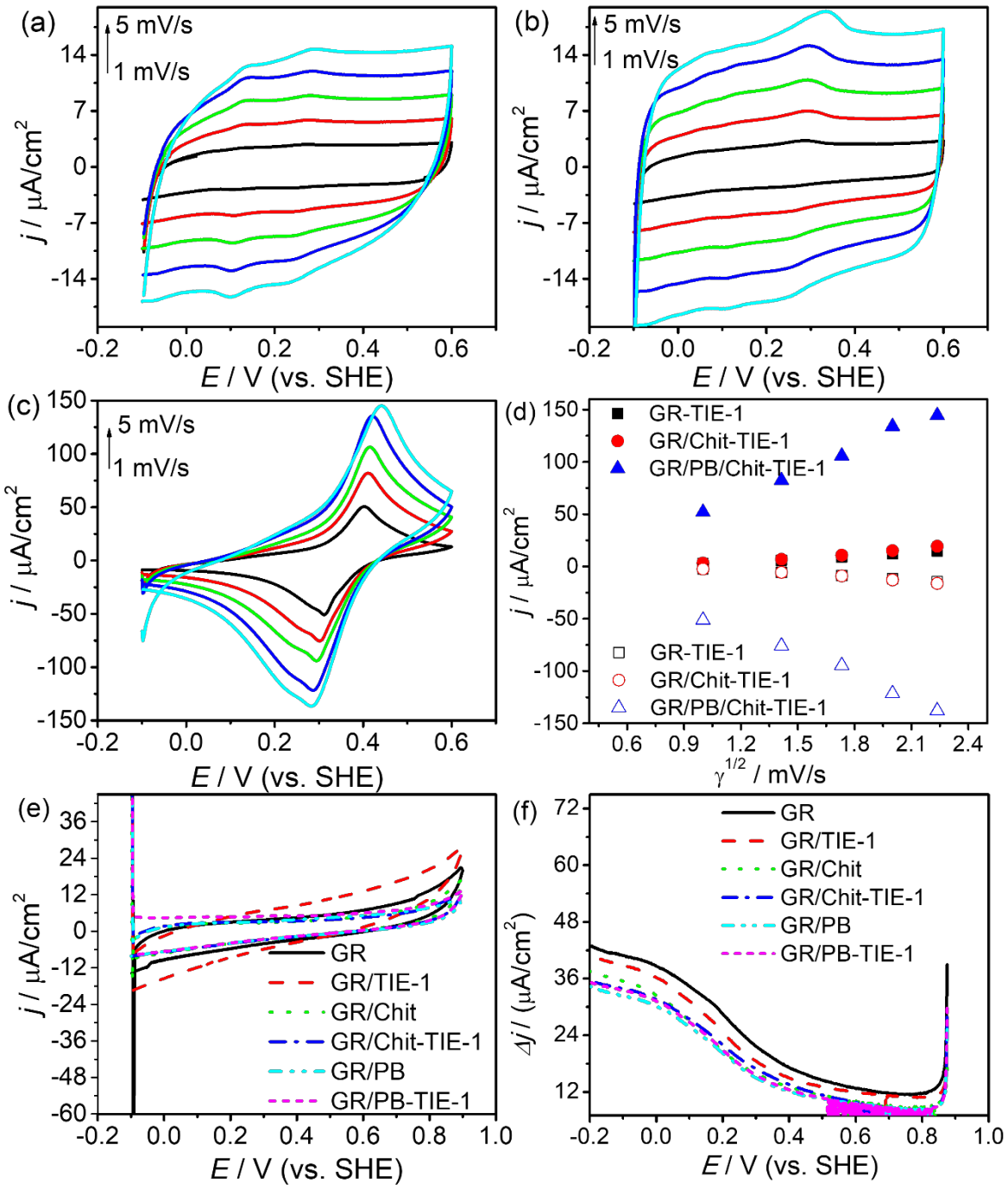
(a)
5 mV/s
1 mV/s
j / μA/cm2
E / V (vs. SHE)
(b)
5 mV/s
1 mV/s
j / μA/cm2
E / V (vs. SHE)
(c)
5 mV/s
1 mV/s
j / μA/cm2
E / V (vs. SHE)
(d)
GR-TIE-1
GR/Chit-TIE-1
GR/PB/Chit-TIE-1
GR-TIE-1
GR/Chit-TIE-1
GR/PB/Chit-TIE-1
j / μA/cm2
γ1/2 / mV/s
(e)
GR
GR/TIE-1
GR/Chit
GR/Chit-TIE-1
GR/PB
GR/PB-TIE-1
j / μA/cm2
E / V (vs. SHE)
(f)
GR
GR/TIE-1
GR/Chit
GR/Chit-TIE-1
GR/PB
GR/PB-TIE-1
Δj / (μA/cm2)
E / V (vs. SHE)

Fig. 6.

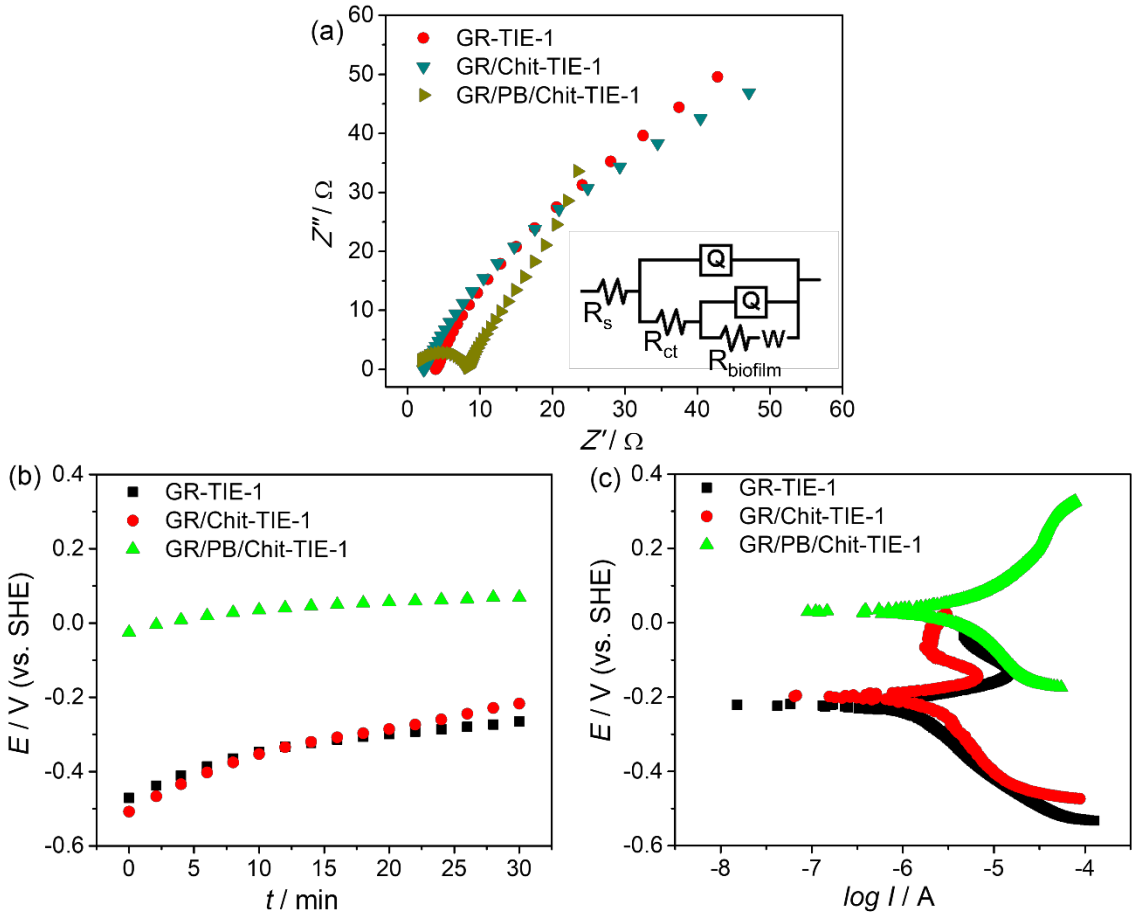
(a)
GR-TIE-1
GR/Chit-TIE-1
GR/PB/Chit-TIE-1
Z'' / Ω
Z' / Ω
Q
Q
Rs
Rct
W
Rbiofilm
(b)
GR-TIE-1
GR/Chit-TIE-1
GR/PB/Chit-TIE-1
E / V (vs. SHE)
t / min
(c)
GR-TIE-1
GR/Chit-TIE-1
GR/PB/Chit-TIE-1
E / V (vs. SHE)
log I / A

Fig. 7.

Supporting Information

An Insoluble Iron Complex Coated Cathode Enhances Direct Electron Uptake by *Rhodopseudomonas palustris* TIE-1

Karthikeyan Rengasamy, Tahina Ranaivoarisoa, Rajesh Singh, Arpita Bose*

Department of Biology, Washington University in Saint Louis, St. Louis, MO, 63130, USA.

*Corresponding author email: abose@wustl.edu, Tel: +1-314-935-7313

Table S1. Ferrozine assay of $FeCl_2$ dissolved medium at the end of 152 h EU experiment.

Systems	Time (h)	Fe (II)		Fe (III)	
		mM	%	mM	%
$FeCl_2$	0	6.32 ± 0.02	100	0	0
$FeCl_2$	152	5.11 ± 0.33	80.83 ± 5.2	1.21 ± 0.17	19.17 ± 2.7
$FeCl_2$ + TIE-1	152	4.07 ± 0.55	64.40 ± 8.6	2.25 ± 0.28	35.59 ± 4.5

Table S2. EIS circuit values derived from $R_s(Q(R_{ct}(Q(R_{biofilm}W))))$

Graphite cathodes with microbe	R_s, (Ω)	Q, (Farad)	R_{ct}, (Ω)	Q, (Farad)	$R_{biofilm}$, (Ω)	W, (Ω)
GR-TIE-1	2.494	0.0073	1.558	0.0077	5143	0.0002
GR/Chit-TIE-1	2.208	0.0086	1.613	0.0012	141.1	0.0009
GR/PB/Chit-TIE-1	1.067	1.03E-5	7.308	0.0133	13.3	0.0113

Table S2. Tafel parameter derived from Tafel plots shown in Figure 7c

Graphite cathodes / microbe	Anodic electron transfer co-efficient (β_a)., mV/decade	Cathodic electron co-efficient (β_a), mV/decade	Exchange current density (I_0), µA	Potential at I=0, mV
GR-TIE-1	281 ± 2.3	587.3 ± 2	1.05 ± 0.02	-271 ± 3
GR/Chit-TIE-1	70.10 ± 1.7	288.9 ± 1.3	1.9 ± 0.02	-247 ± 5
GR/PB/Chit-TIE-1	62.3 ± 2.2	197.2 ± 3.7	10.3 ± 0.07	+45 ± 3

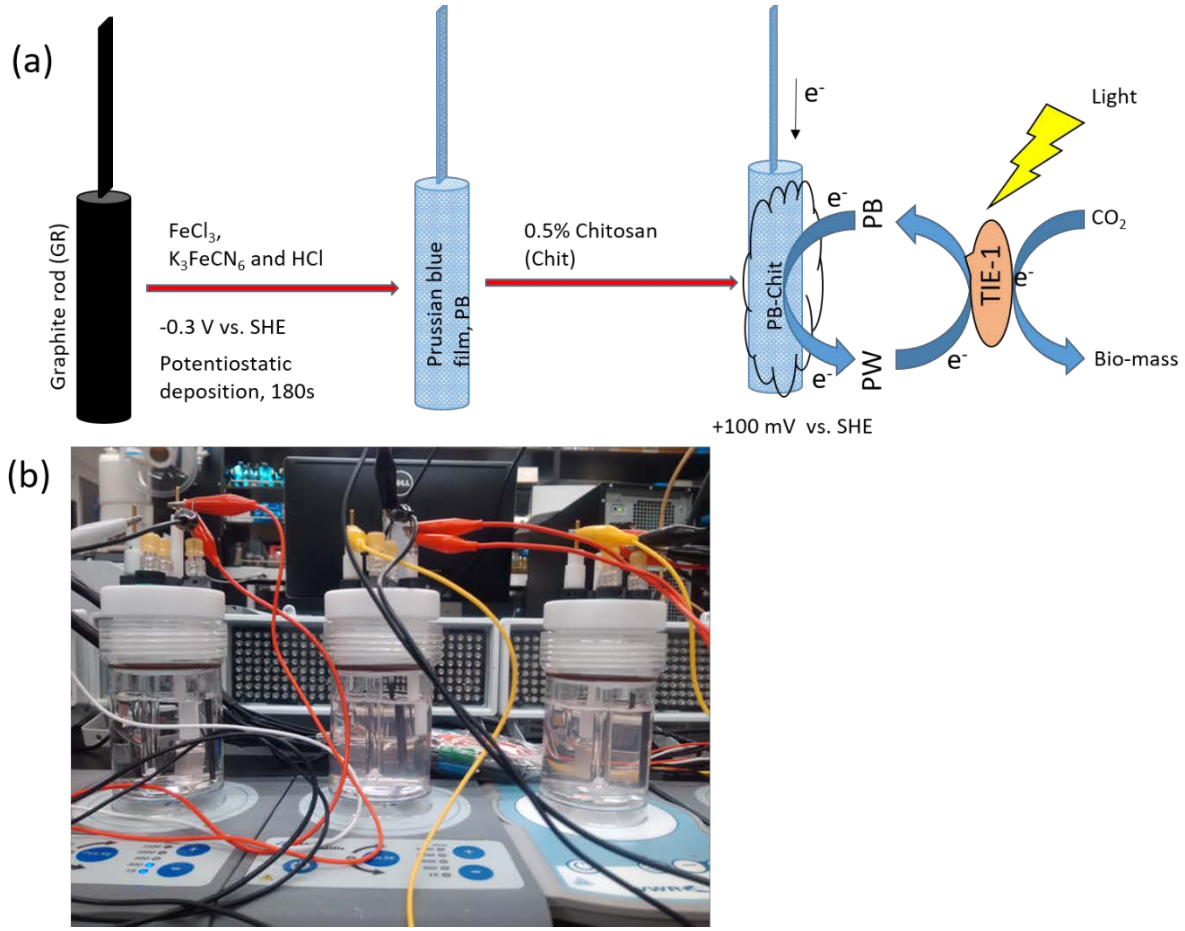

Fig. S1 Schematic representation for the electrochemical deposition of Prussian blue on a graphite rod and the expected microbial reaction (a); Bioelectrochemical experimental setup (b).

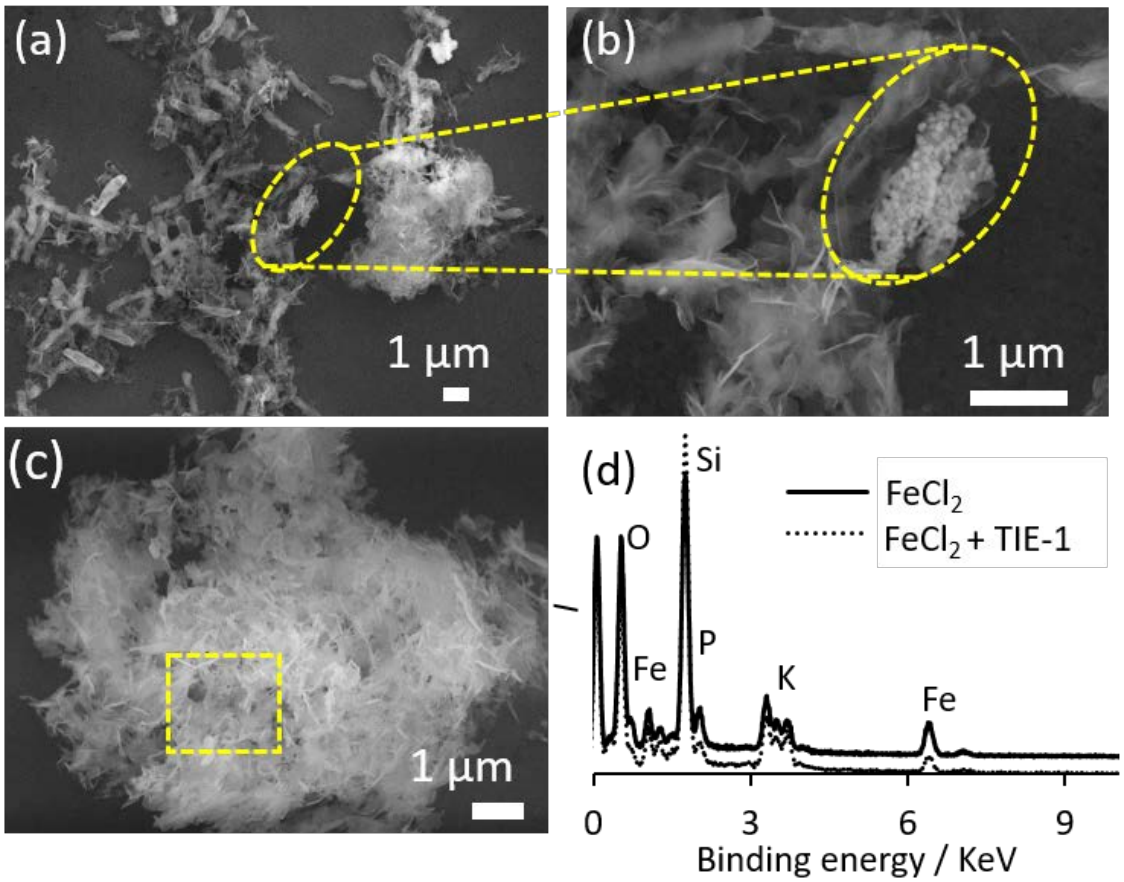

Fig. S2 (a, b) SEM images of spent medium containing planktonic cells coated with amorphous Ferrihydrite in the biotic system ($FeCl_2$ + TIE-1) and (c) abiotic system ($FeCl_2$). (d) EDS (Electron Dispersive Spectroscopy) of portion circled in (a).

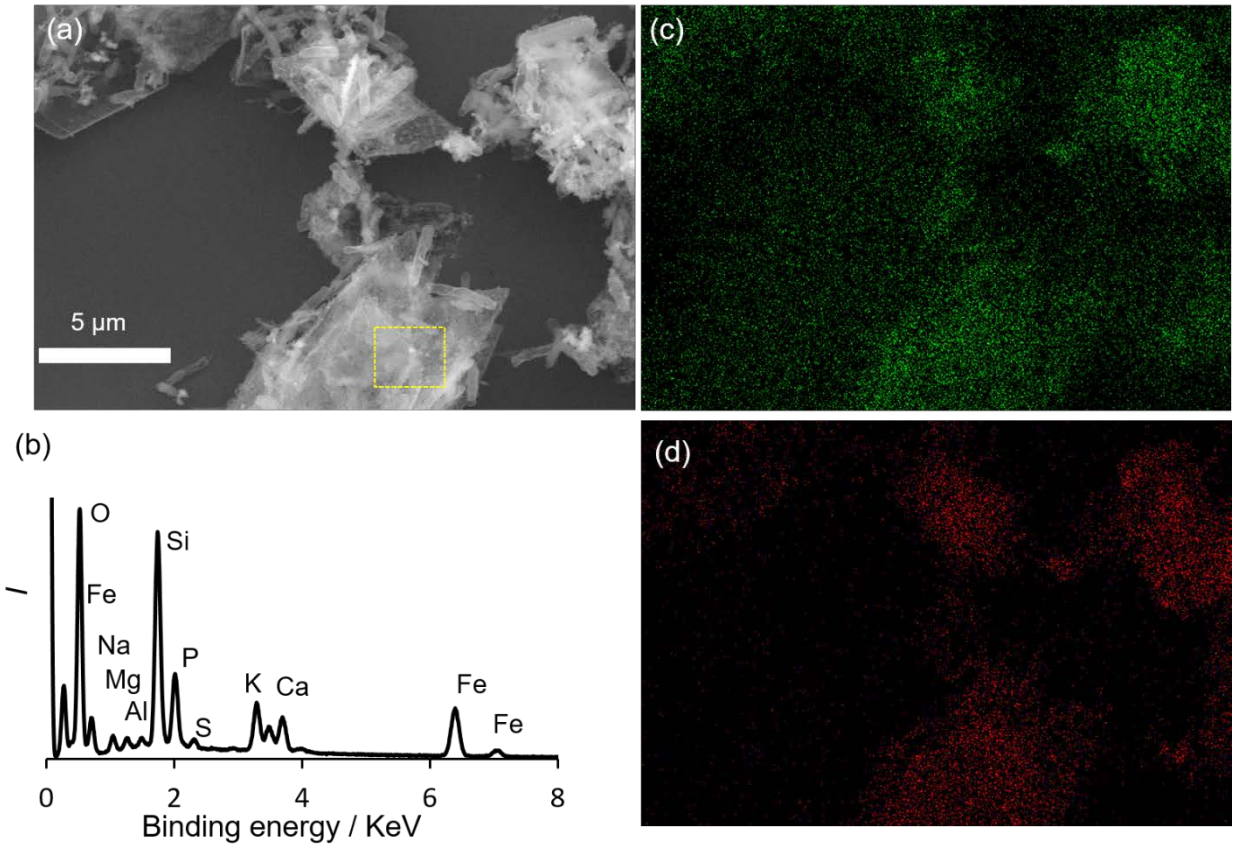

Fig. S3 SEM image of spent medium containing planktonic cells with sheet like Ferrihydrite formation in a biotic reactor where dissolved Fe(II) was added (TIE-1→ $FeCl_2$, biotic system) (a), EDS spectrum corresponds to the yellow square area (b), Elemental map of Oxygen (c), and Iron (d).

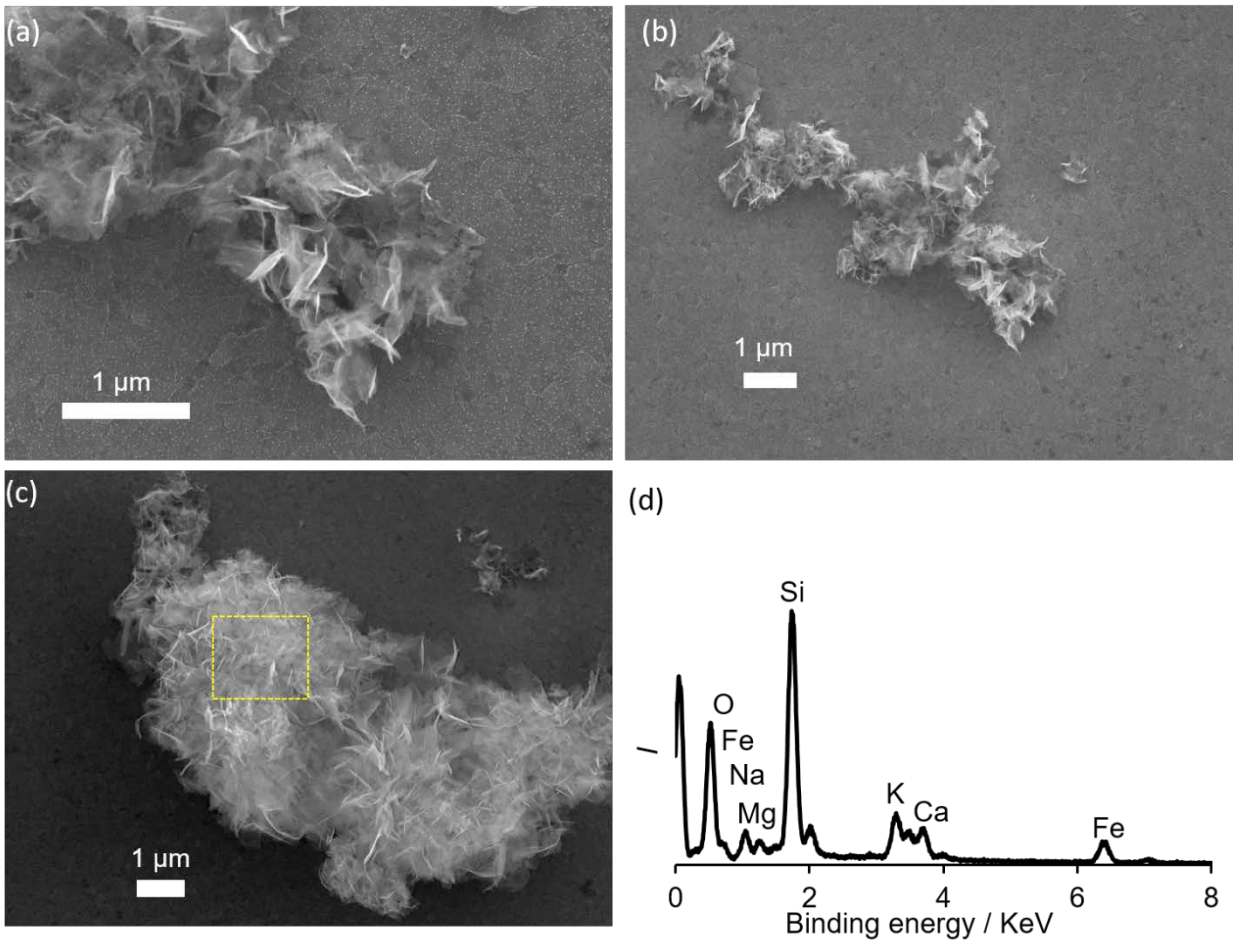

Fig. S4. (a, b, c) Final time point SEM images of Ferrihydrite complex formation in an abiotic reactor ($FeCl_2$, Abiotic) with dissolved Fe(II); (d) EDS spectrum that corresponds to the yellow square area in (c).

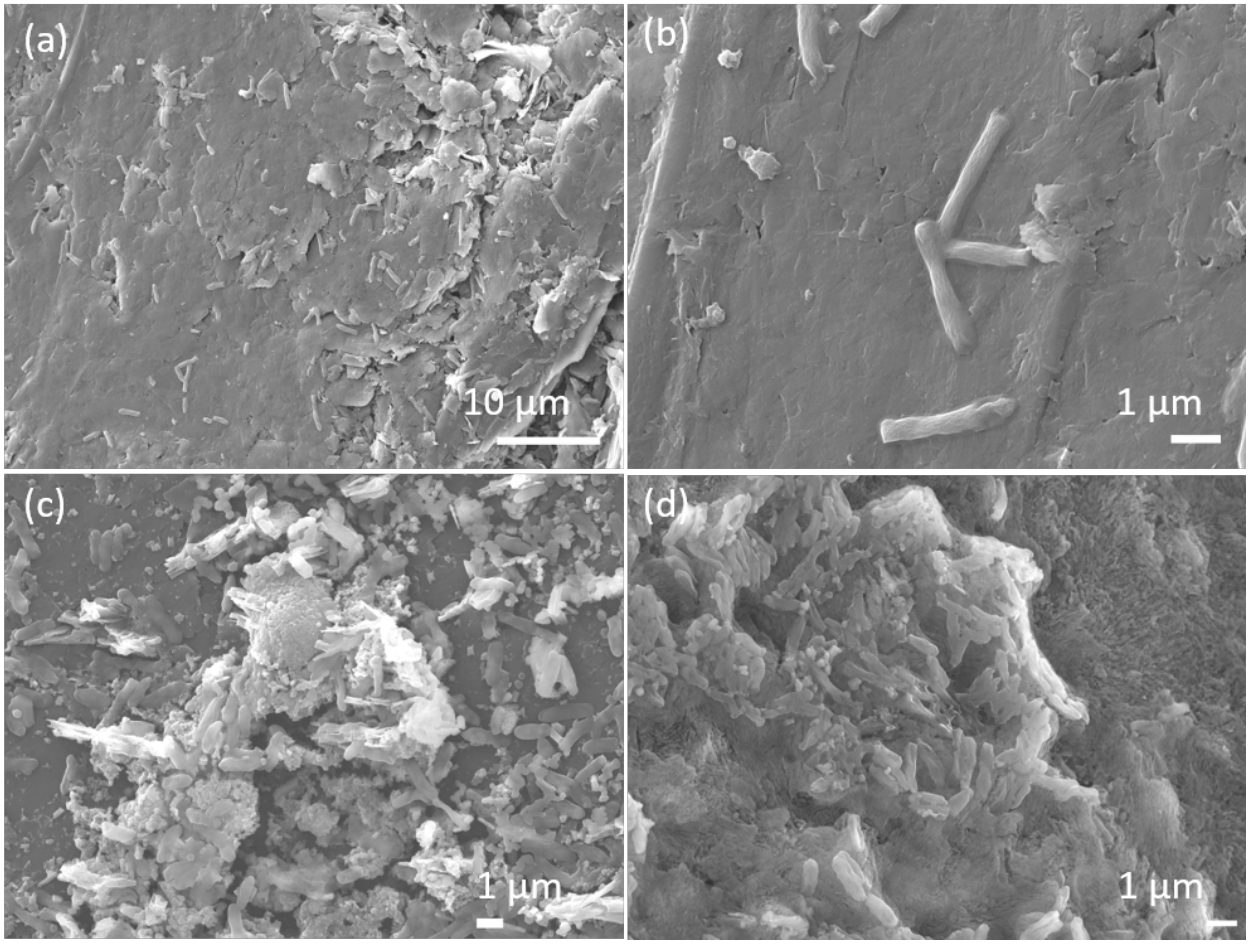

Fig. S5 SEM images depicting attachment of TIE-1 on different graphite electrodes; graphite alone (a, b); biocathodes modified with chitosan (c); and biocathodes modified with PB-Chitosan (d).

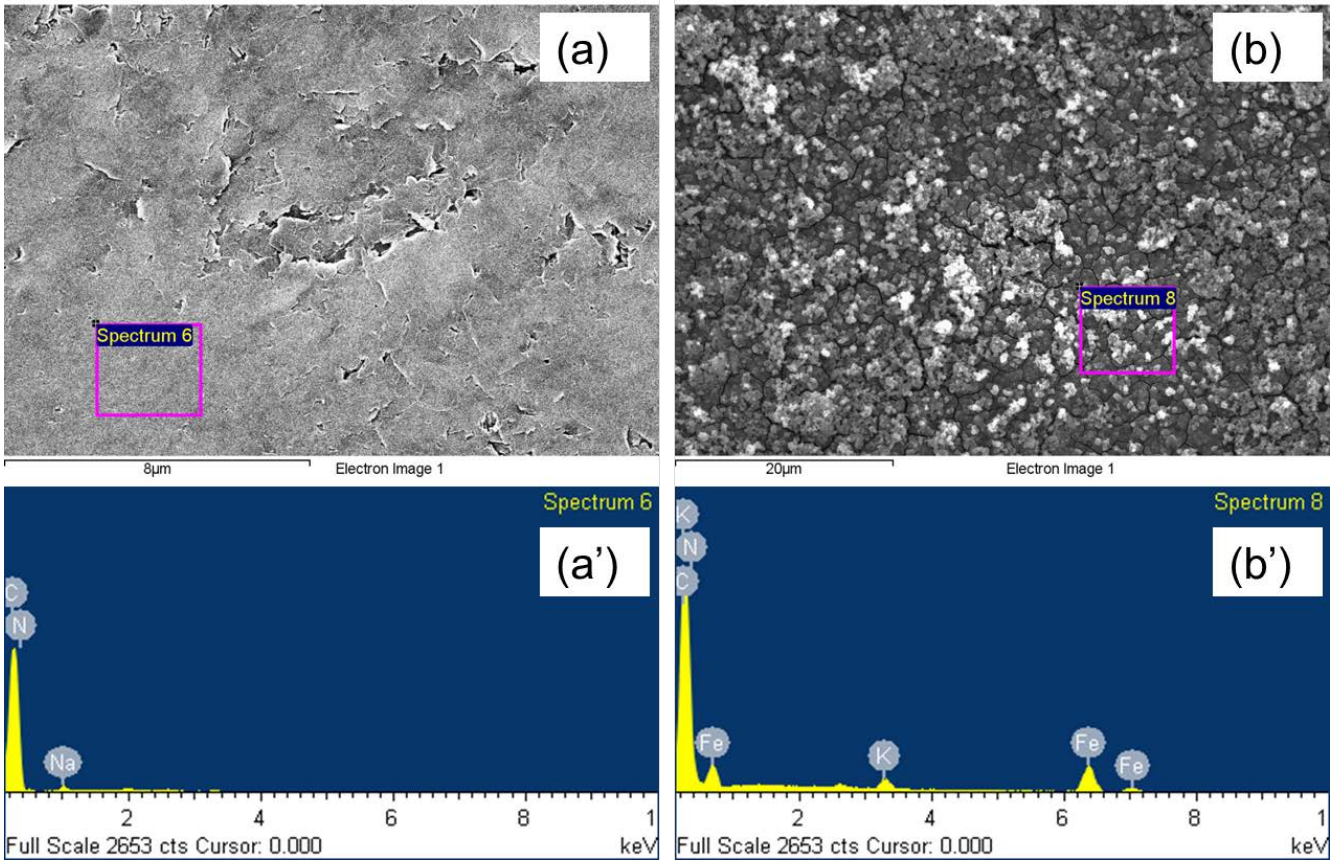

Fig. S6 SEM image of plain graphite electrode surface (a) and Prussian blue (PB) deposited surface (b); EDS analysis of plain graphite electrode (a') and Prussian blue (PB) deposited surface(b'). The characteristic "Fe" elemental peak was observed in the PB deposited electrode surface (b'). This confirms the electrodeposition of PB on the graphite electrode surface.